Energy & Environmental Science

REVIEW

View Article Online
View Journal | View Issue

Lithium metal anodes for rechargeable batteries

Wu Xu,*[a] Jiulin Wang,[ab] Fei Ding,[c] Xilin Chen,[a] Eduard Nasybulin,[a] Yaohui Zhang[ad] and Ji-Guang Zhang*[a]

Cite this: *Energy Environ. Sci.*, 2014, **7**, 513

Received 8th March 2013
Accepted 29th October 2013

DOI: 10.1039/c3ee40795k

www.rsc.org/ees

Lithium (Li) metal is an ideal anode material for rechargeable batteries due to its extremely high theoretical specific capacity (3860 mA h g^{-1}), low density (0.59 g cm^{-3}) and the lowest negative electrochemical potential (−3.040 V *vs.* the standard hydrogen electrode). Unfortunately, uncontrollable dendritic Li growth and limited Coulombic efficiency during Li deposition/stripping inherent in these batteries have prevented their practical applications over the past 40 years. With the emergence of post-Li-ion batteries, safe and efficient operation of Li metal anodes has become an enabling technology which may determine the fate of several promising candidates for the next generation energy storage systems, including rechargeable Li–air batteries, Li–S batteries, and Li metal batteries which utilize intercalation compounds as cathodes. In this paper, various factors that affect the morphology and Coulombic efficiency of Li metal anodes have been analyzed. Technologies utilized to characterize the morphology of Li deposition and the results obtained by modelling of Li dendrite growth have also been reviewed. Finally, recent development and urgent need in this field are discussed.

1. Introduction

Lithium (Li) metal has an extremely high theoretical specific capacity (3860 mA h g^{-1}), low density (0.59 g cm^{-3}) and the lowest negative electrochemical potential (−3.040 V *vs.* the standard hydrogen electrode); thus rechargeable Li metal batteries have been investigated extensively during the last 40 years.[1,2] Unfortunately, rechargeable batteries based on Li metal anodes have not yet been commercialized. There are two main barriers to the development of Li metal batteries. One is the

[a]*Energy and Environment Directorate, Pacific Northwest National Laboratory, Richland, WA 99354, USA. E-mail: jiguang.zhang@pnnl.gov; wu.xu@pnnl.gov*
[b]*Department of Chemical Engineering, Shanghai Jiao Tong University, Shanghai 200240, China*
[c]*National Key Laboratory of Power Sources, Tianjin Institute of Power Sources, Tianjin 300381, China*
[d]*College of Science, Harbin Institute of Technology, Harbin 150001, China*

Dr Wu Xu is a Senior Research Scientist in the Energy and Environment Directorate of Pacific Northwest National Laboratory. He received his Ph.D degree from the National University of Singapore in 2000. His main research interests include the development of novel electrolytes and electrode materials for different kinds of energy storage devices such as lithium (Li-ion, Li–air, Li–metal) batteries, supercapacitors, and organic redox flow batteries.

Prof. Jiulin Wang received his bachelor and master degrees from the Harbin Institute of Technology in 1999, and Ph.D degree from the Shanghai Institute of Microsystem and Information Technology, Chinese Academy of Sciences in 2002; he studied at Tsinghua University and Queen's University (Canada) as a postdoctoral researcher from 2002 to 2004; he joined Shanghai Jiao Tong University as associate professor in 2005 and went to the Chemnitz University of Technology (Germany) as an Alexander von Humboldt fellow for one and a half years; now he is a visiting scholar at PNNL. His main research focuses on nanomaterials for high energy density batteries, especially on Li–S batteries.

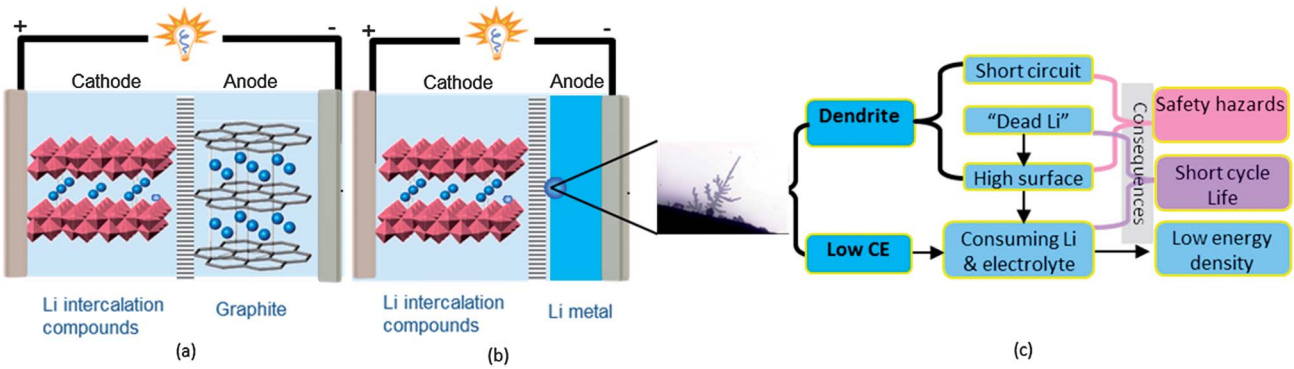

Fig. 1 Schematic diagram of (a) Li ion batteries; (b) Li metal batteries; (c) the typical morphology of Li dendrites and the main problems related to dendrites and low Coulombic efficiency (morphology picture in (c) is reproduced with permission.[3] Copyright 1976, *J. Crystal Growth*).

growth of Li dendrites during repeated charge/discharge processes, and another is the low Coulombic efficiency (CE) of these processes. These two barriers consequently lead to two critical problems for Li anodes – one is safety hazards because of potential internal short circuits and high surface area, and another is short cycle life. Although low Coulombic efficiency can be partially compensated by an excess amount of Li, for example, an excess amount of 300% of Li was a common solution in the early development of Li metal batteries, but the dendrite-growth related battery failure, sometimes dramatic failure that led to fire and other hazards, and the emergence of Li-ion batteries have largely diminished industry's efforts in the development of rechargeable Li metal batteries since the early 1990s.

Fig. 1(a) and (b) show the schematic diagram of a typical Li ion battery and a Li metal battery, respectively. In Li-ion batteries, graphite has been widely used as the anode material because Li ions can be intercalated into its layered structure so that Li dendrite growth can be prevented. In the case of Li metal batteries, the cathode shown in Fig. 1(b) can be replaced with a sulphur (for Li–S battery) or air electrode (for Li–air battery).

Fig. 1(c) shows the typical morphology of Li dendrites and the main problems associated with dendrites and low Coulombic efficiency of the Li deposition/striping process.

With the urgent need for the "next generation" rechargeable batteries, such as Li–S[4,5] and Li–air batteries,[6,7] the use of Li metal anodes has attracted significant interest in recent years. In the last 40 years, Li dendrite formation has been widely analyzed[2,3,8–10] and simulated.[11–13] Most approaches to dendrite prevention focus on improving the stability and uniformity of the solid electrolyte interphase (SEI) layer on the Li surface by adjusting electrolyte components and optimizing SEI formation additives.[8,9,14–16] However, because Li is thermodynamically unstable in organic solvents as indicated by Aurbach *et al.*,[8] it is very difficult to achieve sufficient passivation on Li electrodes in liquid solutions. As an alternative, various mechanical barriers, either *ex situ* coated polymer layers or solid-state blocking layers with high shear modulus, have been proposed to block dendrite penetration.[11,17–21] These approaches rely on a strong mechanical barrier provided by an SEI film or a separator to suppress Li dendrite penetration but do not change the fundamental, self-amplifying behaviour of the dendrite growth. In other words,

Dr. Fei Ding got his Ph.D degree from the Harbin Institute of Technology in 2006. Now he works as a group leader in the China National Key Laboratory of Power Source, Tianjin, China. In the last few years, he focused on the next generation electrochemical power sources, including lithium–air batteries, lithium–sulfur batteries and some other lithium metal rechargeable batteries. Following on from his Ph.D research, he has continued his studies on rechargeable lithium metal anodes for around ten years.

Dr Ji-Guang (Jason) Zhang is a Laboratory Fellow of the Pacific Northwest National Laboratory (PNNL). He is the group leader for PNNL's efforts in the area of energy storage for transportation applications. He has 23 years of experience in the development of energy storage and energy efficient devices, including Li-ion batteries, Li–air batteries, Li–metal batteries, Li–S batteries, thin-film solid-state batteries, and electrochromic devices. He was the co-recipient of two R&D 100 awards, holds 11 patents (with another 14 patents pending) and has published more than 100 papers in refereed journals. Dr Zhang received his Ph.D in Experimental Condensed Matter Physics from the University of Kentucky in 1990.

these methods did not prevent Li dendrites from growing during long-term cycling, or hardly improve the Coulombic efficiency in Li deposition/stripping which is not suitable for practical rechargeable Li batteries.

In this work, we will first briefly review the general models of the dendrite growth mechanisms, and then give more detailed discussions on various instruments/tools that are critical for the investigation of Li dendrite growth. The different approaches to the protection of Li metal anodes used in the past 40 years, including strategies that can suppress Li dendrite growth and the electrolytes that can lead to high Coulombic efficiency during Li deposition/stripping processes will be analyzed. Finally, recent developments and new directions in this field will also be discussed.

2. Modelling of Li dendrites

2.1 General models

In the field of electrodeposition, metal "dendrites" are a common phenomenon. At a given electrodeposition condition, many metals such as Zn, Cu, Ag, Sn, *etc.* were reported to exhibit ramified morphologies.[22] Fractal deposits including needle-like, snowflake-like, tree-like, bush-like, moss-like, and whisker-like structures are all referred to as dendrites in this review. Extensive studies have been done on the dendrite formation mechanism during electrodeposition of Zn and Cu. Various strategies have been unitized to suppress dendrite growth in these processes.[23,24] The reported methods to suppress Zn dendrites include special separators, alternative current or pulsed charging, and additives in the electrolytes. The latter methods can be further divided into three categories: structural modifiers to electrodes, metallic additives, and organic additives.[25] Several factors such as zinc concentrations, complexing agents, anions, and additives may modify the texture and morphology of zinc electrodeposited coatings.[26] Recently, Aaboubi *et al.*[27] investigated the effect of tartaric acid on zinc electrodeposition from sulphate plating bath by electrochemical impedance spectroscopy, stationary polarization curves, X-ray diffraction (XRD) and SEM imagery. The study shows that it is possible to obtain homogeneous, compact and dendrite-free zinc deposits from sulphate solutions containing tartaric acid. Abe *et al.*[28] also reported suppression of the dendrite formation in metallic zinc deposition using zinc oxide electrodes modified with an anion-exchange ionomer (AEI). These improvements are explained by the selective ion permeation through the AEI films. These approaches towards Zn dendrite suppression and the techniques used in the investigation of Zn dendrite growth are useful for the investigation and prevention of Li dendrite growth.

Although most electrodepositions are a one-time-only process, Li metal in a rechargeable Li metal battery needs to be plated on or stripped from substrates repeatedly during charge/discharge processes. Therefore, Li dendrites will accumulate on the anode and finally lead to many serious problems (see Fig. 1) which hinders the practical applications of rechargeable Li metal batteries. Therefore, a good understanding of the mechanism of Li dendrite formation and growth is critical to mitigate or further eliminate Li dendrites.

Many groups have simulated the Li dendrite formation and growth process, and proposed several meaningful and fundamental models in the last forty years. In order to simplify the simulation conditions, most models were based on a binary electrolyte with a Li salt and polymer electrolyte, for example, $LiClO_4$ or $LiN(SO_2CF_3)_2$ (LiTFSI) in polyethylene oxide (PEO). Under the open circuit condition, the electrolyte is in a steady state without an ionic concentration gradient; under polarization, the Li^+ and the anion will diverge and transfer to the negative and positive electrodes, respectively. Li^+ will obtain an electron and plate on the negative electrode. The speed of Li deposition or consumption of Li^+ depends on the applied current density. Although the depletion of Li^+ can be macroscopically compensated by the supply of Li^+ from the positive electrode, the microscopic ionic distribution near the negative electrode dramatically affects the deposit's morphology. Therefore, a basic model to simulate Li dendrites starts from the calculation of the concentration gradient in the Li symmetric cell under polarization. Brissot and Chazalviel *et al.* described the concentration gradient in a cell with a small inter-electrode distance using the following equation,[29,30]

$$\frac{\partial C}{\partial x}(x) = \frac{J\mu_a}{eD(\mu_a + \mu_{Li^+})} \quad (1)$$

where J is the effective electrode current density, D is the ambipolar diffusion coefficient, e is the electronic charge, μ_a and μ_{Li^+} are the anionic and Li^+ mobilities. From eqn (1), two different conditions for a symmetrical Li/PEO/Li can be anticipated, with the inter-electrode distance L and the initial Li salt concentration C_o.

(a) If $dC/dx < 2C_o/L$, the ionic concentration evolves to a steady state where the concentration gradient is constant and varies almost linearly from $C_a = C_o - \Delta C_a$ at the negative electrode to $C_{Li^+} = C_o + \Delta C_{Li^+}$ at the positive electrode, where

$$-\Delta C_a \approx -\Delta C_{Li^+} \approx \frac{\mu_a}{\mu_a + \mu_{Li^+}} \frac{JL}{eD} \quad (2)$$

(b) If $dC/dx > 2C_o/L$, the ionic concentration goes to zero at the negative electrode at a time called "Sand's time" τ, which varies as,

$$\tau = \pi D \left(\frac{eC_o}{2Jt_a} \right)^2 \quad (3)$$

$$t_a \approx 1 - t_{Li^+} = \frac{\mu_a}{\mu_a + \mu_{Li^+}} \quad (4)$$

where t_a and t_{Li^+} represent the anionic and Li^+ transference number, respectively. Brissot and Chazalviel *et al.* indicated that the anionic and Li^+ concentrations exhibit different behaviours at the Sand's time, leading to an excess of positive charge at the negative electrode. This behavior will result in a local space charge, form a large electric field, and lead to nucleation and growth of Li dendrites. The results of their simulations and experiments confirmed the concentration gradient and the occurrence of dendrites very close to the Sand's time.[31,32] Chazalviel also predicted that the dendrites will grow at the velocity of

$$v = -\mu_a E \quad (5)$$

where E is the electric field.[22]

Monroe and Newman developed the general model describing dendrite growth under galvanostatic conditions applicable to liquid electrolytes.[33] They adopted the Barton and Bockris method[34] with the addition of thermodynamic reference points and the fact that the concentration and potential are not constant during the course of dendrite growth. They calculated the concentration and potential distribution in the cell at different time intervals. It was demonstrated that the dendrite growth rate increases across the electrolyte and depends greatly on the applied current density, which will be discussed in more detail in the following section.

Rosso *et al.* reported a systematic study on the evolution of Li dendrites in the PEO–LiTFSI electrolyte involving theoretical calculations as well as experimental data.[29] They demonstrated that even though the formation of dendrites has little effect on the overall impedance, it significantly decreases the interfacial impedance. Based on the impedance data, the value of resistance due to the dendrites could be calculated. In addition, it was observed that dendrites can burn out like a fuse, *i.e.*, when the first dendrite reaches the opposite electrode it shorts the circuit and the current density passing through this single dendrite becomes high enough to melt it. Thus, the final short circuit occurs only when the major front of dendrites eventually reach the opposite electrode.

Although the formation of contiguous and conducting Li dendrites in batteries is often called 'dendritic growth', there are actually several modes of formation and growth: dendrites, whiskers, and 'others'. The true dendrite grows from a Li–metal surface in a non-aqueous electrolyte by adding material to its tip. The nutrient source is the Li in the electrolyte. Classical models of dendrite growth gave solutions in the form of the tip radius times its velocity, which has the units of diffusivity. Recent electrochemical continuum models[35] and experiments[36] on Li batteries have found that the dendrite growth is controlled by the tip surface energy, which always accelerates across the cell under all conditions, and can be partially mitigated by lowering the limiting current or increasing the cell thickness. The latter two conditions limit the performance of the battery. A second type of growth has been simulated in some Li battery experiments. If the nutrient supply is drawn from the Li–metal sheet, growth occurs at the base of a 'whisker'. Yamaki[37] analyzed the stress-assisted whisker growth through cracks in a protective layer (*i.e.* the separator) on the surface of the Li anode.

2.2 Effect of current density

It is well known that the effective current density during Li deposition/stripping has a significant impact on the dendrite formation and growth. Generally, low current density results in a relatively stable cycling and conversely high current density accelerates the invalidity process of rechargeable Li metal batteries. The equation of Sand's time indicates that the dendrite initiation time is proportional to J^{-2}, which indicates that high current density greatly accelerates the formation of Li dendrites. It is worth noting that there are some results showing $\tau \sim J^{-1}$.[25] rather than $\tau \sim J^{-2}$ dependence, as reported by Liu *et al.*[38] They attributed this deviation to the local fluctuations of the current density. Moreover, the ionic liquid used in their work acted as a supporting electrolyte. In fact, this is a ternary electrolyte rather than a binary one as assumed by Chazalviel's model. In the model developed by Monroe and Newman[33] using a liquid electrolyte, the tip growth rate (v_{tip}) can be expressed as

$$v_{tip} = \frac{J_n V}{F} \quad (6)$$

where J_n is the effective current density normal to the dendrite (hemispherical) tip, V is the molar volume of Li and F is the Faraday's constant. This equation suggests that the dendrite growth rate is proportional to J_n. Based on eqn (3) and (6), the dendrite initiation time could be delayed and the dendrite growth rate could be slowed down if the effective current density could be decreased. By applying a smaller current density, a smoother surface and improved cycling life have been obtained.[9,39–43]

According to Chazalviel's model, an applied current density leads to an ion concentration gradient; high current density results in a near zero ion concentration at the negative electrode and the formation of Li dendrites at Sand's time; low current density leads to a minimal and stable ion concentration gradient so no Li dendrites form under this condition. The crossover between the two regimes is the limiting current density

$$J^* = 2eC_o D/t_a L \quad (7)$$

When the current density is low, there is in principle no Sand behavior and the concentration variation should be small. However, experimental results clearly indicate that there are still Li dendrites, but not as many as at high current density. Rosso *et al.*[35] and Teyssot *et al.*[44] attributed the formation of dendrites to the local non-uniformity of the Li/electrolyte interface which leads to a large concentration variance even in the depleted zone close to the conditions of Chazalviel's model. Brissot *et al.*[31] confirmed this experimentally in a Li|PEO–LiTFSI|Li cell although individual dendrites could deviate from the predicted growth rate. It was demonstrated that at high current densities (when Li deposition becomes diffusion controlled), the onset of dendrite formation matched that at Sand's time (zero ion concentration). However, dendrites started to grow earlier with cycling, apparently because of the created defects. At low current densities (*i.e.*, when concentration variations were low), dendrites were also observed in the form of elongated metal filaments (higher aspect ratio), which could be a result of local inhomogeneity. Growth velocities followed Chazalviel's model[22] in both cases. It was later shown by Rosso *et al.* that the time of dendrite appearance at low current densities is also proportional to the power of current density even though Sand's behavior was not expected.[35] It was proposed that the specific properties of the PEO–LiTFSI electrolyte cause destabilization of the concentration distribution along the electrode surface. A direct relationship between

dendritic growth and concentration gradient was clearly demonstrated by employing three independent techniques to measure ion concentrations in the vicinity of dendrites.[32]

In addition to the values of current density, the charge styles, galvanostatic or pulse, also significantly affect Li dendrite formation and growth. Recent work by Miller and co-authors reported that pulse charging can effectively suppress Li dendrite formation by as much as 96%. They proposed a coarse-grained lattice model to explain the mechanism of pulse charging and revealed that dendrite formation emerged from a competition between the timescales of Li^+ diffusion and the reduction at the anode, with lower over-potential and shorter electrode pulse durations shifting this competition in favor of the lower dendrite formation probability.[45]

2.3 Importance of interfacial elastic strength

Monroe *et al.* further employed the linear elasticity theory to develop a kinetic model describing how mechanical properties of polymer electrolytes (shear modulus and Poisson's ratio) affect the roughness on the Li interface.[11] The interface was subjected to a regime of small-amplitude two-dimensional (2D) perturbations. Analytic solutions with specific boundary conditions allowed computation of deformation profiles. Compressive stress, deformation stress and surface tension at the elastic Li interface were calculated as the next step. Incorporation of these parameters into the model gave a prediction of the distribution of exchange current density along the electrode surface. Finally, it was possible to verify that the mechanical properties of the polymer electrolyte stopped amplification of the dendrite growth. It turned out that dendrite suppression can be achieved when the shear modulus of the electrolyte is about twice that of the Li anode ($\sim 10^9$ Pa), *i.e.*, at least three orders of magnitude higher than that of the studied PEO.

As in many other fields, all of the models discussed above have their limitations. For example, the dendrite growth velocity proposed by Monroe and Newman[33] (see eqn (6)) was derived from the growth of a single dendrite without considering the interactions among neighbouring dendrites. It was also stated that the Chazalviel theory[22] has limited applications in real batteries because it applies at currents higher than the limiting current. However, Rosso *et al.*[35] and Teyssot *et al.*[44] made a conclusion that the Chazalviel model can be extended to low currents due to the nanoscale inhomogeneity in the concentration, at least in the case of PEO-based electrolytes. Even though these models still include many simplifications and limitations, they have established a solid foundation for the nucleation and growth mechanism of dendrites. More importantly, as we will discuss later in this review, several general predications of these models have been used successfully to identify new approaches to suppress dendrite growth, especially during Li metal deposition, for example, using an anode with a large surface area to reduce the effective current density, developing a single ion conductor to enhance the Li^+ transference number, developing an electrolyte with strong shear modulus, and adding a supporting electrolyte. These approaches will be discussed in detail in Section 4.

3. Li dendrite characterization

As discussed above, dendrite growth during the Li deposition process that occurs during battery charging is a critical issue for battery safety. In the last 40 years, extensive work has been done to characterize the nucleation, formation, and growth processes of Li dendrites in order to reveal the mechanisms of dendrite growth. The techniques used to study Li dendrite formation include scanning electron microscopy (SEM), optical microscopy, atomic force microscopy (AFM), nuclear magnetic resonance (NMR), Fourier transform infrared spectroscopy (FTIR), X-ray photoelectron spectroscopy (XPS), and several other methods. Actually, all these methods can be categorized as the morphology study and the chemical composition study of the Li surface.

3.1 Surface morphology characterization

Morphology studies focus on the variations of the Li surface and formation of Li dendrites. Among various observation methods, SEM is the most useful technique that can directly reveal the high resolution details of Li dendrite growth. Therefore, it has been used extensively to analyse changes in the surface morphology of Li metal during the deposition and stripping processes since the 1970s.[9,13,15,46–51] The effects of solvents,[46,49,52–54] salts,[47,48,55] additives[14–16,56,57] and other treatments[51,58,59] have been revealed directly from the SEM images. With SEM, the correlation between the surface chemistry and the morphology of Li electrodes was established,[47] and morphological transitions in the Li metal anode during cycling were clearly identified.[50] Most previous SEM investigation on Li dendrite growth has been done *ex situ*, *i.e.*, deposited samples were disassembled from electrochemical cells and transferred to the SEM instrument chamber with minimum exposure to air as described by Kohl and co-workers.[51] Orsini *et al.*[60,61] further improved this method by designing a removable load lock chamber to transfer a sample from a glove box to the SEM without exposing the sample to air. They also used a Li metal battery with polymer electrolytes (PEs) to replace conventional batteries which contain more liquid electrolytes. This approach enabled them to observe the cross-sections of cells and minimize the effect of liquid electrolytes on SEM. Their study identified the accumulation of mossy Li and growth of dendritic Li at the Li/PE interface (see Fig. 2), which was the origin of rapid interface deterioration and capacity fading. However, their study in the late 1990s was performed on a cell cut with a razor blade after cycling instead of during the operation of the cell. This is still far from the *in situ* or *operando* spectroscopy developed in recent years. Because of the high vacuum conditions required in the SEM test, it is also difficult to conduct an *in situ* observation of Li dendrite formation and growth in the cells using conventional liquid electrolytes, which is actually more interesting for practical applications.

Optical microscopy is another way to observe Li dendrites and can be used as an *in situ* method to observe and record the Li dendrite growth process. Although the resolution of optical microscopy is not as high as that of SEM, it still could easily and

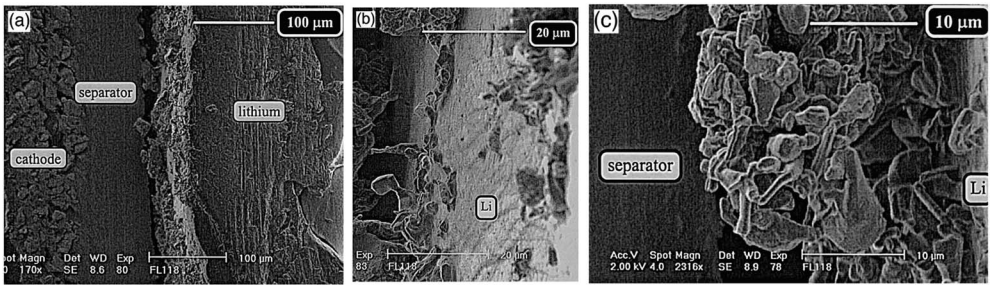

Fig. 2 (a) Cross-section of a Li battery after one charge at 1 C; (b) surface of the Li anode of a Li battery after one charge at 1 C; (c) Li deposit on the Li surface after one charge at 1 C. The 1 C rate was 2.2 mA cm^{-2} (reproduced with permission.[60] Copyright 1998, Elsevier).

instantaneously identify the surface change and dendrite formation. It is an intuitionistic observation on Li electrodes and helpful for understanding a continuous dendrite growth process. With digital recording devices, the dendrite formation process can be recorded on videos. Therefore, the optical microscopy technique has also been widely used to analyze Li electrodes *in situ*. Brissot *et al.*[31] designed a special optical cell for the *in situ* optical study on Li dendrite growth. The optical cell could work as an air-tight electrochemical cell, and the Li electrode surface could be observed by optical microscopy. In the *in situ* observation, optical microscopy is more often used to study the Li surface from the parallel direction to investigate the dendrite growth process.[30,31,62] This setup can also be used to perform an *ex situ* study of the Li surface. The effects of different electrolytes[63] and additives[64] on Li dendrite growth have been investigated using this approach. However, the relatively low resolution of optical microscopy makes it difficult to observe the initial nucleation and development of small Li dendrites grown on the Li surface as clearly as with SEM.

AFM is a useful technique to investigate the Li electrode morphology as well.[2,65–68] The resolution of AFM is much better than that of optical microscopy. At the same time, AFM can give a three-dimensional (3D) morphology image that is impossible for both SEM and optical microscopy. In 1996, Aurbach and Cohen suggested and proved the applicability of AFM to the study of Li deposition processes in nonaqueous electrolyte systems.[2] In that work, the basic electrochemical cell used in AFM was modified to hold the highly sensitive electrodes and electrolyte solution and to isolate them from atmospheric contaminants. It has been found that the AFM scanning is not destructive and does not change the morphology of the surface. With the special 3D morphology of AFM images, the swelling and shrinking of the Li surface during the deposition and stripping processes have been discovered.[68] Fig. 3 shows the AFM images of a Li surface film, where a bump after Li deposition (a) and shrinkage after consecutive Li dissolution (b) are clearly observed.[68] Moreover, the investigation by AFM revealed the structure of the Li surface, consisting of grain boundaries, ridge lines, and flat areas,[65] which are difficult to identify by other morphology test methods including SEM and optical microscopy. Based on these findings, Aurbach *et al.*[28,67] have proposed the breakdown and reparation of the SEI films on Li electrodes during Li deposition/stripping cycles as shown in Fig. 4.[2,67]

Recently, an *in situ* transmission electron microscopy (TEM) technique has been used to observe the Li fiber or Li dendrite growth on anodes in nanoscale Li-ion batteries.[69,70] Huang *et al.* first reported the direct observation of Li fiber growth on different nanowire anodes (such as silicon or tin oxide) during *in situ* charging of nanoscale Li-ion batteries inside a TEM.[69] Li fibers up to 35 μm long grew on nanowire tips along the nanowire axis in an ionic liquid (IL)-based electrolyte. Yassar *et al.* also used the *in situ* TEM technology to study the growth of Li dendrites.[70] They reported the clear observation of nucleation

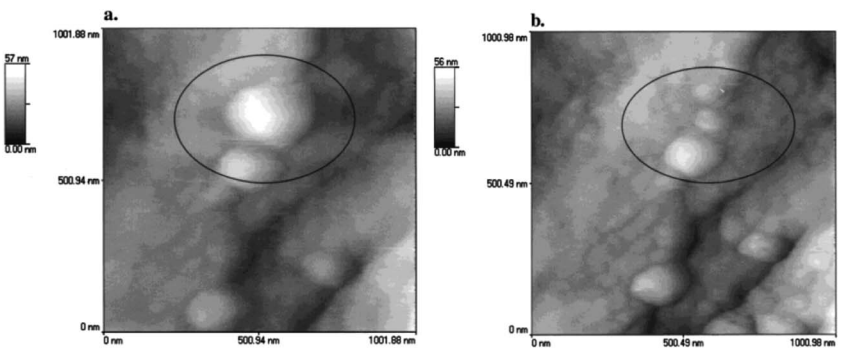

Fig. 3 AFM images (1 × 1 μm) of a Li electrode in a 0.5 M $LiAsF_6$/propylene carbonate (PC) solution. (a) An image obtained after Li deposition, 0.41 C cm^{-2}. New Li deposits are marked by a circle; (b) an image of the same area after consecutive Li dissolution (0.41 C cm^{-2}). The same area marked in (a) is also circled here (reproduced with permission.[67] Copyright 2000, American Chemical Society).

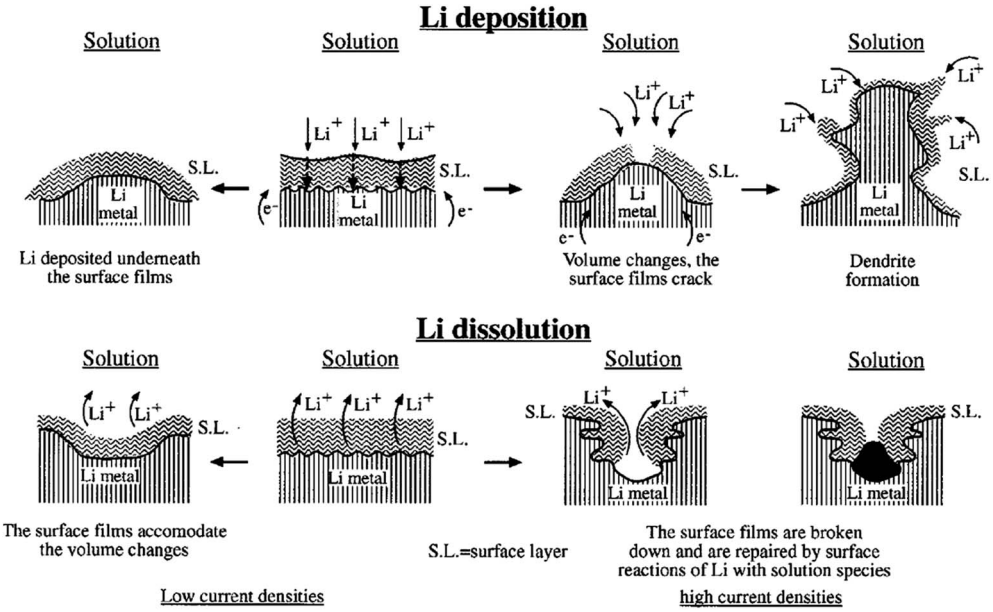

Fig. 4 A description of the morphology and failure mechanism of Li electrodes during Li deposition and dissolution describing selected phenomena: the beginning of dendrite formation and non-uniform Li dissolution accompanied by breakdown and reparation of the surface films (reproduced with permission.[67] Copyright 2000, American Chemical Society).

of Li ions at the anode/electrolyte interface and the growth of Li fibers or Li dendrites on the anode surface in a nanoscale Li-ion battery (see Fig. 5). Although *in situ* TEM is a very promising method to investigate the formation and growth of Li dendrites during the continuous charging/discharging processes of a battery, the current *in situ* TEM studies on Li metal and Li-ion batteries use an IL electrolyte or even a solid-state electrolyte because the high vapor pressure of a practical liquid electrolyte is detrimental to a TEM system. In this case, the interaction between Li dendrites and the practical liquid electrolyte still cannot be identified by these studies. Therefore, there is an urgent need to develop *in situ* TEM techniques that can hold electrochemical cells with a liquid electrolyte so that a true *operando* TEM investigation on Li dendrite growth can be performed.

NMR is a powerful tool for detecting the chemical bonds or atomic surroundings. Recently, Bhattacharyya and Grey *et al.* proposed using the difference between NMR signal intensities of bulk and porous Li to identify the Li dendrite growth.[36] They have successfully used this method as an *in situ* tool to quantitatively observe the formation of Li dendrites in different electrolytes. Chandrashekar *et al.*[10] recently reported using a ^{7}Li magnetic resonance imaging (MRI) technique to detect *in situ* the variation of Li electrode morphologies during the charge and discharge processes of a symmetric Li metal cell. The schematic cell design and its orientation with respect to the static magnetic field in the NMR spectrometer are shown in Fig. 6(a). The ^{7}Li NMR spectra of the Li metal resonance before (pristine) and after applying a current (charged) shown in Fig. 6(b) indicated that the area of the spectrum in the charged state was 2.3 times larger than that in the pristine state. This increase could be attributed to the formation of dendritic, mossy and other microstructural metallic Li during charging.

The 2D ^{7}Li MRI images before and after the cell charging are depicted in Fig. 7(a) and (b), where the cumulative signals were projected along the *z* direction in Fig. 6(a). The MRI image of the

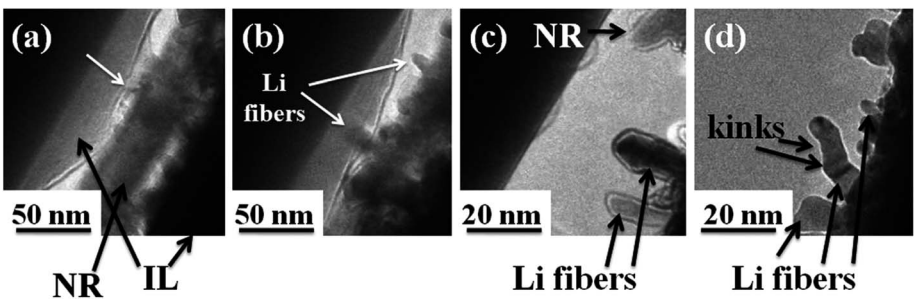

Fig. 5 (a) Black arrows indicate an individual silicon nanorod surrounded by IL. (b) Arrows indicate the formation of Li islands on the nanorod. (c) The growth of Li fibers is represented. (d) The formation of kinks and growth of Li fibers are marked by black arrows (reproduced with permission.[70] Copyright 2011, American Institute of Physics).

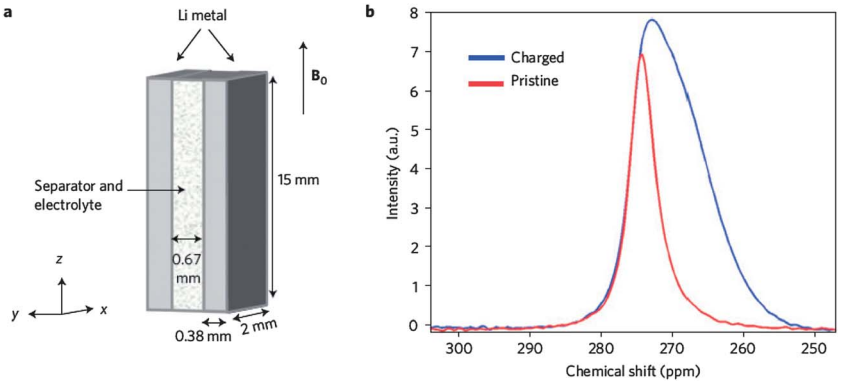

Fig. 6 (a) Schematic structure of a symmetric Li bag cell; (b) comparison of one-dimensional ^{7}Li NMR spectra in pristine and charged states (reproduced with permission.[10] Copyright, Nature).

charged battery revealed that the negative electrode had a significant increase in signal of almost double, while the positive electrode showed a signal decrease of about 23% after charging. It indicated the location and change of microstructural Li morphology, which is consistent with findings from SEM images Fig. 8(c) and (d). It is seen that MRI can also give some useful information about the Li dendrite morphologies.

3.2 Surface film analyses

Besides the morphologies of Li electrodes, another important work in the study of Li anodes is to analyse the chemical compositions of the surface films. As mentioned before, Li metal is thermodynamically unstable in organic solvents; Li instantaneously reacts with a solvent to form an electrically insulating and ionically conductive interface which physically prevents the direct contact between Li and the solvent, therefore making Li dynamically stable in some organic solvents. This electrically insulating and ionically conductive interface was first named as the solid electrolyte interphase (SEI) by Peled in 1979.[71] The chemical composition of an SEI layer is related to the electrolyte composition (including salts, solvents, and additives) and strongly affects the Li morphology and cycling performance of a Li battery.[47] The possible chemical reactions that occurred on the Li surface could be deduced from the chemical compositions of the SEI layer. In these studies, FTIR and XPS are the most important technologies for analysing the Li surface chemistry; FTIR is more suitable for detecting the organic components while XPS gives more information about the inorganic components.

From the locations and strengths of the peaks in FTIR spectra, different chemical bonds or components on the Li electrode surface could be identified. Since the 1980s, FTIR has been widely used as a non-destructive method to analyse the Li surface.[68,72–75] In the beginning, FTIR was used as an *ex situ* method,[72] but it has also been developed into an *in situ* technique for analysing Li surface films during electrochemical processes.[68,75] The influences of electrolyte solvents, salts,

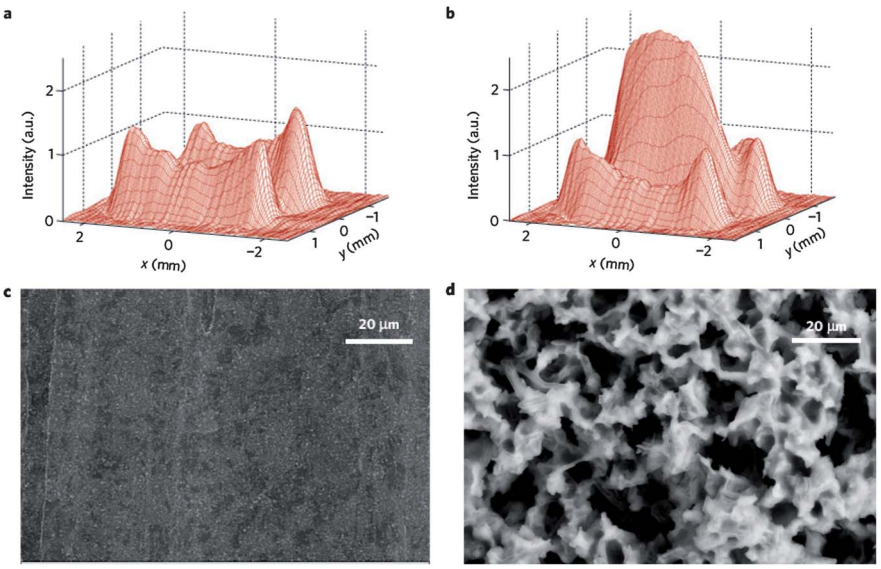

Fig. 7 ^{7}Li 2D MRI x–y images (the frequency encoding in x and the phase encoding in y) in the pristine (a) and after-charging (b) states, and the related SEM images of a Li anode in pristine (c) and charged (d) states (reproduced with permission.[10] Copyright, Nature).

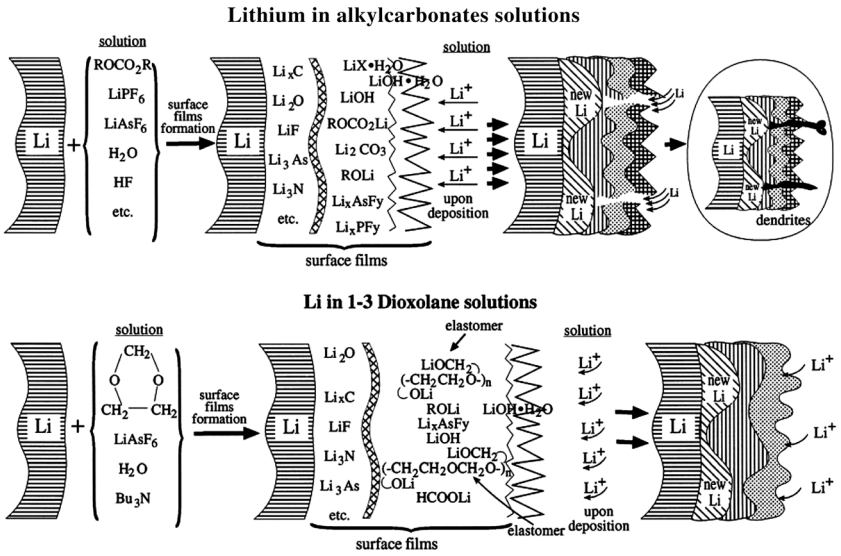

Fig. 8 A schematic illustration of surface film formation on Li electrodes in alkyl carbonates and in DOL solutions (reproduced with permission.[103] Copyright 2000, Elsevier).

additives and other contaminants on the Li surface chemistry have been systematically investigated *via* FTIR. Aurbach *et al.* have detected the FTIR peaks on Li surfaces and deduced the possible components on Li surfaces.[47,53,74] Based on these composition data, Aurbach *et al.* also proposed some possible chemical reactions between Li metal and electrolytes.[53,73]

It should be noted that although the FTIR technique is very useful for identifying the surface components, it detects only the infrared-active species and it cannot give comprehensive information for all surface components and compositions that affect the Li deposition morphology and battery performance. Therefore, other surface characterization methods and technologies besides FTIR are needed to get more-detailed surface chemistry data on Li anodes. As mentioned above, XPS is another very useful tool for analysing the surface chemistry of Li electrodes, especially because it gives more information about the elemental or inorganic components that FTIR cannot detect because they have low or no infrared activity. From the XPS and FTIR data, Aurbach *et al.* found that the major species on Li surfaces include Li_2O, LiOH, LiF, Li_2CO_3, Li alkylcarbonate (RCOOLi), and hydrocarbons.[72] These techniques were also used to identify the effects of different electrolyte solvents,[49,76,77] Li salts[48,56] and additives[15,78] on the Li surface chemistry. Based on these data, not only the components but also the structural composition evolution of the SEI films have been revealed.[15,48,76]

In addition to the technologies discussed above, Raman spectroscopy,[63,79,80] Auger electron spectroscopy (AES)[49,65,74,76] and NMR[44] have also been used to analyze the Li surface chemistry. So far, attempts to use Raman spectroscopy to identify the surface films on Li/electrolyte interphases have not been very successful.[79–82] Irish and coworkers used a Raman microprobe to do *in situ* and *ex situ* studies on the surface films formed on Li metal in contact with electrolytes of $LiAsF_6$ in tetrahydrofuran (THF) and 2-methyltetrahydrofuran (2Me-THF). The reaction products detected were mainly polytetrahydrofuran, some arsenolite (As_2O_3) and arsenious oxyfluorides ($F_2As–O–AsF_2$). It seems that Raman technology could provide results similar to those obtained by FTIR spectroscopy, but Raman technology is more complicated to use than FTIR.[78] In addition, as indicated by Naudin *et al.*,[82] local heating of the samples under laser irradiation is unavoidable in Raman tests. The carbonate species on a Li surface would be transformed into Li acetylides of Li_2C_2 type which give a vibration peak for C≡C at about 1845 cm^{-1}, thus giving a faulty result and leading to a wrong interpretation. Therefore, the destructive effect of the Raman laser beam on a Li surface limits its use in the analysis of Li surface films.

Aurbach *et al.*[76] used AES to measure the Li surface with sputtering after the Li was immersed in an electrolyte of 0.2 M $LiAsF_6$ in 1,2-dimethoxyethane (DME) for 15 min followed by pure DME rinsing. They found that the AES picture was similar to that seen with XPS. Carbon and oxygen were detected at the Li surface. With sputtering, the intensity of the carbon Auger peak decreased while that of the oxygen peak increased when compared to their initial peaks. It was suggested that the surface films of Li in DME consisted of two layers, the upper layer being an alkoxide film (probably $LiOCH_3$) and the layer close to Li being a mixture of Li_2O and LiOH. Kominato *et al.*[83] also used AES to detect the surface compounds of Li after immersion in three electrolytes of ethylene carbonate (EC)/dimethyl carbonate (DMC) with $LiPF_6$, $LiClO_4$ and $LiN(SO_2CF_3)_2$ (LiTFSI), respectively. Except for LiF found in the Li surface film from the $LiPF_6$-based electrolyte, all major components on the Li surface were Li–O components including LiOH, Li_2O or other Li oxide compounds. Morigaki and Ohta[65] used scanning AES to analyze the Li surface in 1 M $LiClO_4$/PC solution. Li_2CO_3, Li_2O and LiOH were localized on the ridge lines and the grain boundaries of the Li surface. Similar to XPS, AES technology could also give some useful information about the Li surface components.

The use of NMR to study the Li surface chemistry is even less common. Ota *et al.*[49] used NMR technology (^{1}H, ^{13}C and 2D spectra) to analyze the surface components of the deposited Li by dissolving the surface film in anhydrous dimethyl sulfoxide-d_6 (DMSO-d_6) and then recording the NMR spectra of the organic species in the DMSO-d_6 solution. They found that the organic surface layer on Li metal included Li ethoxide, Li ethylene dicarbonate, and Li ethylene containing an oxyethylene unit. However, solution NMR is an indirect method to analyse the Li surface focusing on the dissolvable organic species, and it is limited to analysis of the insoluble inorganic compounds formed on Li surfaces. In this case, solid NMR with magic angle spinning might be more suitable for detecting Li interfacial components and functional groups.

Nazri and Muller utilized secondary ion mass spectrometry (SIMS) to study the surface layer formed on electrochemically deposited Li on copper in a 1 M $LiClO_4$/PC electrolyte.[84] The obtained SIMS spectrum was complex and more difficult to interpret than those obtained from other techniques such as FTIR, Raman and XPS. The low-mass range showed fragments of PC, salt and water, while the high-mass range indicated the presence of a polymeric material based on PC, a partially chlorinated hydrocarbon polymer and their Li adducts. The authors also applied an *in situ* X-ray diffraction technique to analyse the film on a Li surface and identified the formation of Li_2CO_3, Li_2O and some polymers.[84–86]

Temperature-programmed decomposition mass spectroscopy and gas chromatography-mass spectrometry (GC-MS) technology have also been used to analyse the surface components of Li electrodes.[83] In these measurements, the Li electrodes with SEI need to be heated to generate the gases to be detected. Kominato *et al.*[83] reported that the gases generated from Li films pretreated in EC–DMC-based electrolytes were composed mainly of CH_4, H_2O, CO, CH_3OH, CO_2 and ethylene oxide (EO). N_2 was also detected if $LiN(SO_2CF_3)_2$ was used as the electrolyte salt. These results indicate that the detected gases were generated from the organic Li compounds, including Li ethylene dicarbonate and Li methylcarbonate that were the reaction products of Li and solvents, EC and DMC. Ota *et al.*[87] also used GC-MS to investigate the Li surface compounds generated in EC/THF electrolytes. The detected gases consisted mainly of C_2H_4, CO_2 and C_2H_6 produced by decomposition of EC. The data from these MS measurements could bring additional information on the composition of the Li surface film and are complementary to the information obtained from FTIR and XPS.

Kominato *et al.*[83] and Ota *et al.*[87] utilized ion chromatography (IC) to quantitatively analyse the Li surface films. The Li films were first dissolved in high-purity water and then tested using an IC instrument. By analysing the contents of F^-, CO_3^{2-} and Li^+ ions, quantitative information about the Li surface films could be obtained. Ota *et al.*[87] found that the Li surface film in EC-based electrolytes consisted mainly of Li alkyl carbonate, and the LiF content in the films in Li imide salt electrolytes was lower than those in the $LiPF_6$ electrolyte.

Besides the above surface morphology and chemical composition analyses, another promising technology for Li surface characterization is the *in situ* scanning vibrating electrode technique.[88,89] This *in situ* technology could map the surface electric field on the Li electrode. Based on the models proposed by Chazalviel and optimized by Brissot, under polarization, a concentration gradient and ionic heterogeneous distribution form an electric field in the rechargeable Li batteries. It is this electric field that induces the formation of Li dendrites and determines their growth rate at a velocity $v = -\mu_a E$, where μ_a is the anionic mobility and E is the electric field. The *in situ* scanning vibrating electrode technique can experimentally detect not only the surface morphology but also the chemical composition uniformity of the Li surface, which approximately determine the start time of Li dendrite formation and its growth rate. However, because the scanning step of this technology is not small enough, extensive optimization is needed before adopting it to precisely detect the electric field on a Li surface. Electrochemical techniques, *i.e.*, galvanostatic cycles and polarization measurement, are the most simple and practical methods for investigating the Li dendrite growth. Balsara *et al.* investigated Li dendrite growth in a symmetric Li cell that is expected to be more rapid than in a battery with a Li metal anode and an intercalation cathode. After a certain number of cycles, the sharp drop in the magnitude of oscillating voltage indicates the formation of a short dendrite.[90]

As we discussed above, different analytical techniques provide different information on the morphologies and surface components of Li anodes, but any one of them is not enough to get a comprehensive understanding of the Li surface, especially for the interfacial reaction products or SEI chemistry. SEM provides qualitative information with adjustable magnification, and quantitative and spatial information can be obtained *via* NMR and MRI. A combination of characterization and analysis techniques is required to provide a good understanding of the morphology and composition of the deposited Li film. Among these techniques, the most commonly used techniques include SEM, FTIR, and XPS, which provide the basic information on the properties of deposited Li films. New methods, for example a miniature liquid cell *via operando* TEM, might be much more suitable for the observation of Li deposition from liquid electrolytes.

4. Li dendrite prevention

4.1 Li dendrite prevention by *in situ* formed stable SEI film

The SEI at the electrode/electrolyte interphase was first proposed by Peled in 1979 after he and others studied nonaqueous batteries using alkali and alkaline earth metals as anodes.[71] This layer (15–25 Å thick) instantly formed on the metal surface when the metal contacted the nonaqueous electrolyte. It consists of some insoluble products from the reactions of the metal and the electrolyte, and acts as an ionically conductive but electronically insulating layer like a solid electrolyte. Currently the SEI concept has also been extended to all electrode surface layers including graphite anodes and metal oxide cathodes.

The SEI film forms immediately on the Li surface once the Li metal is soaked in a nonaqueous electrolyte or electrodeposited

from a nonaqueous electrolyte.[8,91–94] As an anode for a rechargeable battery, Li will be plated and stripped during charge/discharge processes. During the charging process, the formation of a Li dendrite and its growth leads to a significant increase in surface area and a large amount of fresh Li metal is exposed to the organic electrolyte. The high metal-solution potential difference causes several reduction processes involving reduction of solvents, salts and all the usual atmospheric contaminants at potentials about 1 V higher than that of the Li/Li^+ couple.[95,96] This process is called "self-remedying" of SEI which instantaneously re-stabilizes the Li metal anode. However, repeated SEI formation consumes both Li metal and electrolyte, which requires excess Li to compensate the Li loss and leads to drying up of the electrolyte. It also results in a continued increase in cell resistance and poor Coulombic efficiency of the batteries. In the worst case, a large increase in surface area leads to safety hazards, including fire or explosions. Therefore, the quality of the SEI is critical for the feasibility of Li anodes used for rechargeable batteries. An ideal SEI should possess high Li ionic conductivity, dense film, small thickness and high elastic strength to mechanically suppress the breakthrough by Li dendrites. The components and structures of the SEI are determined by the organic solvents, Li salt types and additives as discussed in the following sections. The importance of the SEI and its dependence on the components of the nonaqueous electrolyte have been well documented before, especially in Xu's comprehensive review.[97] Here we focus on its impact on the Li dendrite formation and growth.

4.1.1 Effect of organic solvents. The solvents are the source of organic Li salts in SEI films. Aurbach *et al.* found that the major surface species formed on Li are $(CH_2OCO_2Li)_2$ in EC, $CH_3CH–(OCO_2Li)CH_2OCO_2Li$ in PC, CH_3OLi and CH_3OCO_2Li in DMC, HCOOLi in methyl formate (MF), $CH_3CH_2OCO_2Li$ and CH_3CH_2OLi in diethyl carbonate (DEC), $CH_3(CH_2)_2COOLi$ in γ-butyrolactone, $ROLi(CH_3(CH_2)_3OLi)$ in THF, Li pentoxides in 2MeTHF, $ROLi(CH_3OLi)$ in DME, $CH_3CH_2OCH_2OLi$ and HCO_2Li in 1,3-dioxolane (DOL); EC reduction products dominate in EC–PC or EC–DEC mixtures, HCO_2Li and/or $ROCO_2Li$ species dominate in mixtures containing MF, and $ROCO_2Li$ dominates in EC or PC with ethers.[72,74,98–100] The presence of moisture could convert $(CH_2OCO_2Li)_2$ to Li_2CO_3.[74] The inorganic salts formed in SEI films are mainly determined by the salts used in the electrolytes.[91,101] For example, LiF and Li_xAsF_x formed in SEI when $LiAsF_6$ was used as the salt; Li_2O, LiCl, $LiClO_3$, and $LiClO_2$ formed when $LiClO_4$ was used; LiF and Li_xPF_x formed when $LiPF_6$ was used.[74]

While the imperfection (disordered structure) of the SEI layer endows it with ionic conductivity,[102] the resistance of the SEI layer continues to increase with its thickness and the reduction of solution species becomes more selective.[95] Moreover, the outer layer of the SEI film close to the solution is porous and non-uniform because the reduction of solution species cannot take place over the entire film-solution interface but rather in certain locations of holes and defects through which electron injection is possible when the film grows to a certain thickness.[95] Therefore, the chemical composition and the physical structure of the film change gradually from the interface of Li/SEI to the interface of SEI/solution.[95,96] The film stops growing when it is thick enough to block electron transfer. The minimum thickness of the SEI film is about several tens of Angstroms, determined by the tunnelling range of the electrons in the SEI and by a mechanism of dielectric breakdown of the SEI.[91] Close to the Li surface, the surface films consist mainly of species of low oxidation states such as LiO, LiN, Li halides and lithiated carbon moieties. The outer part of the surface films is comprised of species of higher oxidation states, such as $ROCO_2Li$, ROLi, LiOH, Li_xMF_x (M = As, B, P, *etc.*), $RCOO_2Li$, *etc.*

The surface films are more heterogeneous in their chemical structure, leading to more non-uniform Li deposition and, therefore, dendrite formation as shown in the upper part of Fig. 8.[103] This dendrite formation was the major failure mechanism when Li metal was used as the anode for rechargeable batteries. Due to the breakdown of the surface film in the Li deposition or stripping, the fresh Li surface is exposed to and reacts with electrolyte solutions to form new SEI films. The repeated breakdown and reparation of the SEI films lead to consumption of solution, and therefore low cycling efficiency and short cycle life.[101,103] The dendrite also can short the battery and cause a severe safety issue.

Many organic solvents have been studied for the Coulombic efficiency in Li–metal–anode-based batteries. The cycling efficiency of a Li metal anode was reported to be less than 85% in PC,[104–106] 88% in THF,[107–109] an average of 96% in 2MeTHF,[109–112] 97% in polymethoxy ethers[113] and dimethoxy propane,[114] 98% in diethyl ether,[109,115] less than 85% in DME or ethyl glyme and less than 50% in diglyme,[116] above 96% in DOL,[52,117–120] and about 80% in ILs.[121–126] However, Li cells using electrolytes with the aforementioned solvents (except DOL) show poor capacity retention[115,127,128] and internal short circuits due to dendrite growth.[129] Only the electrolyte with DOL as a solvent and $LiAsF_6$ as a salt shows prolonged cycling stability. This is because the reduction of DOL generates oligomers of polydioxolane.[52] The polydioxolane oligomers are insoluble and adhere to the Li surface with their intrinsic alkoxy (OLi) edge groups.[103] These elastomers (polydioxolane oligomers) endow the SEI films with more flexibility than SEI films formed in other electrolyte solutions as illustrated in the lower part of Fig. 8. This flexible SEI film can accommodate the morphological/volume change of the Li metal during cycling and thus suppress dendrite formation, leading to good cycling life for rechargeable batteries with Li metal anodes.

Fig. 9 shows the typical cycle life behavior of $Li|LiMnO_2$ rechargeable AA cells developed by Tadiran.[120] The cells were tested at 100% and 50% depth of discharge (DOD) ($I_{discharge}$ = 330 mA, and I_{charge} = 60 mA) and they demonstrate good cyclability in 500 cycles at 50% DOD.[52,117–120] Adding EC or PC to the DOL electrolytes can improve the uniformity of the SEI[117] and the homogeneous Li deposition and stripping. It will also increase the Coulombic efficiency of the process. However, this long cycle life was gained at a slow charge rate (*ca.* C/13) and half depth of charge/discharge. Quick charging and deep cycling will still lead to Li dendrite growth and short circuit of the cells.

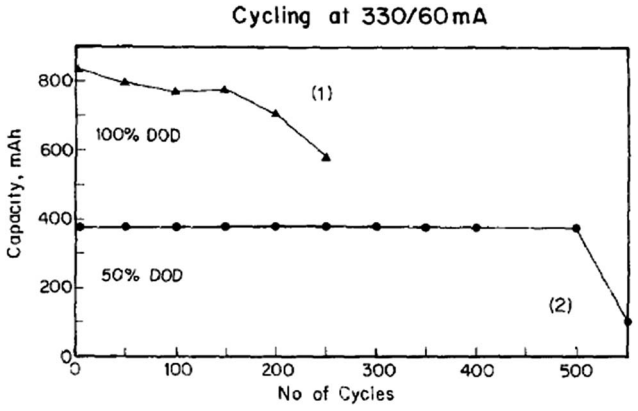

Fig. 9 Typical cycle life behaviour of the Tadiran $LiMnO_2$/Li rechargeable AA cells at 100% and 50% DOD, $I_{discharge}$ = 330 mA, and I_{charge} = 60 mA (reproduced with permission.[120] Copyright 1997, Elsevier).

4.1.2 Effect of Li salts. Besides the effect of solvents, Li salts in nonaqueous electrolytes also play a critical role in the cycling efficiency of Li metal anodes since the surface chemistry of a Li metal anode is strongly affected by the reduction of the salt anions. As discussed above, the inner layer of the SEI film close to the Li metal surface consists mainly of inorganic salts which are dominated by the reduction products of anions in salts if no additives or contaminants exist. If a salt can react with Li metal and form a thin, compact and uniform SEI film, the dendrite growth could be suppressed and thus high cycling efficiency of a Li metal anode would be achievable if paired with a suitable solvent. A salt used in an electrolyte for a Li metal rechargeable battery should meet the following criteria: (1) high chemical stability and compatibility with Li anode and the cathode; (2) wide electrochemical window; (3) high safety and low toxicity; (4) good ionic conductivity in solution.[47]

Compared to the variety of solvents, the available Li salts are very limited. Dahn and coworkers investigated over 150 electrolyte solvent compositions but only five Li salts were suitable for rechargeable Li batteries.[130] Aurbach and co-workers studied the influence of Li salts, such as Li halides, $LiBF_4$, $LiPF_6$, $LiSO_3CF_3$ and LiTFSI, on the behaviour of Li electrodes in THF and PC solutions. They found that $LiBF_4$, $LiPF_6$, $LiSO_3CF_3$, and LiTFSI salts are more reactive with Li (therefore adversely affecting the Li cycling efficiency) than $LiClO_4$ and $LiAsF_6$.[47,131–133] The nonreactive salts, such as LiBr, $LiClO_4$ and $LiAsF_6$, tend to form a stable and thin SEI on the Li surface; in contrast, the reactive salts, such as $LiBF_4$, $LiPF_6$, $LiSO_3CF_3$, and LiTFSI, may result in thick interface films, and some of these films even grow during storage and lead to increased resistance.[134] However, $LiPF_6$ does show higher cycling efficiency than $LiClO_4$ and $LiBF_4$ in dimethyl sulfoxide-DME or sulfolane-DME solvent, as reported by Matsuda.[133]

Naoi and co-workers reported a salt, Li bis(perfluoroethylsulfonylimide) ($LiN(C_2F_5SO_2)_2$, LiBETI), which can form a very stable, thin, uniform, and compact surface film containing mainly the LiF component and consequently give a slightly higher cycling efficiency than $LiPF_6$, LiTFSI, or $LiCF_3SO_3$ in EC/DME solvents.[54] The concentrations of salts also affect the cycling efficiency of the Li anode. As indicated by the Sand model, "Sand's time" is proportional to $C_{Li^+}{}^2$, which means that high Li^+ concentration can delay the start time for Li dendrite formation. This conclusion is valid within a certain range of salt concentrations before the viscosity of the electrolyte dramatically increases and the ionic conductivity seriously decreases. For example, the cycling efficiency increases from 72% to 85% if the concentration of $LiAsF_6$ in PC increases from 0.5 M to 1.5 M.[135] A similar phenomenon was also observed by Ogumi and co-workers for the LiBETI/PC electrolyte.[136] As discussed in the modelling Section 2.1,[29,30] the formation and growth of Li dendrites are induced by the Li^+ shortage in the vicinity of the negative electrode. A higher salt concentration provides more Li^+ supply during the charging process so Li dendrite growth can be suppressed significantly in the high-concentration salt solutions.[136] A recent work by Suo *et al.* is an extreme example of this salt concentration effect.[137] When an ultra-high Li salt concentration of up to 7 M was used in Li–S batteries, Li dendrite growth in these batteries was significantly suppressed by this "solvent-in-salt" electrolyte and the battery cycle life was greatly improved. Of course, too high a salt concentration will lead to increased cost and weight so an optimized salt concentration needs to be identified for practical applications.

4.1.3 Effect of functional additives. Since the number of Li salts is very limited and the salts are also required to be as stable as possible, the electrolyte additives with higher reduction voltages than solvents and salts are often used to enhance the SEI films on the Li surface. These additives may react quickly with the Li anode and form a dense interphase that is more stable than those formed by organic solvents and Li salts, therefore minimizing further reactions between Li and electrolytes. The presence of additives and sometimes contaminants, even at the ppm level, can modify the Li surface chemistry in solutions and thus strongly affect the Li cycling efficiency.

(1) CO_2/SO_2: the presence of CO_2 can increase the Li cycling efficiency considerably.[47,74,95,135,138–143] The carbonates formed due to the presence of CO_2 show a band at 1082 cm^{-1} in Raman spectra[140] and pronounced peaks around 1500–1450 and 880–870 cm^{-1} in FTIR spectra.[138] Li_2CO_3 is an efficient passivating agent because it is the least hygroscopic compound of all other possible surface species formed, and the Li_2CO_3 film is highly stable and protective on Li in most nonaqueous solvents used in rechargeable Li batteries.[74] The interfacial impedance of Li electrodes in solutions containing CO_2 is lower than that in solutions without CO_2 and remains constant during storage.[95] Although the depositied Li in CO_2-containing solutions has a highly dendritic nature, these dendrites are efficiently passivated by Li_2CO_3 and remain in intimate contact with bulk Li because of the protection of the Li_2CO_3 layer.[74,138] SO_2 was also tried as an additive for Li electrodes.[144] Similar to CO_2, SO_2 reacts with Li to form a surface film on the Li electrode. The major effect of SO_2 is on the cycling efficiency. However, the passivation film generated from the reaction between SO_2 and Li is ineffective in protecting Li from attack by the electrolyte. Moreover, the toxic property of SO_2 also limits its wide applications for practical batteries.

(2) Hydrogen Fluoride (HF): the Li particles deposited from HF-containing electrolytes have a smooth hemispherical shape.[15] The smooth Li surface is covered by a thin, compact surface film consisting of a bilayer structure of LiF/Li_2O, which is independent of the type of carbonate electrolytes.[15,39,145–147] The Li cycling stability is significantly extended to hundreds of cycles with the presence of a small amount of HF in the electrolyte. However, this surface film affects the morphology of Li particles produced by the subsequent deposition and accumulates during cycling. The accumulated thick film inhibits the supply of HF to the Li surface, leading to dendrite growth. Therefore, the functions of HF additive degrade with cycling.[15,147]

(3) 2-Methylfuran (2Me-F) and related additives: in the 1980s, Abraham *et al.* found that the performance of Li/TiS_2 became worse after removing the impurity 2Me-F (0.2–0.4 volume percentage) from the electrolyte solvent 2Me-THF.[148] It turns out that 2Me-F is a good electrolyte additive and is able to form a surface film through a chemical ring-opening[149] reaction/polymerization to prevent or slow down direct chemical reactions at the Li surface.[150] Though the composition of the surface film remains unclear, the 2Me-F additive increases the conductance of the surface film and contributes to the improved Coulombic efficiency of Li in the electrochemical deposition/stripping processes.[150,151] Li/TiS_2 cells using THF/$LiAsF_6$ plus 0.5 volume percentage 2Me-F can be charged/discharged for 100 cycles as opposed to seven cycles in cells without 2Me-F, but cells still failed in the end due to the shorts caused by formation of dendrites.[148] Other related additives with similar functionalities include furan, 2,5-dimethyl-furan, 2,5-dimethyl-thiophene, 3,4-dihydrofuran, 2-methyl-tetrahydrofuran and 2,5-dimethyl-tetrahydrofuran, which have at least one unsaturated center.[131,152]

(4) Vinylene carbonate (VC) and fluoroethylene carbonate (FEC): VC is another important additive with an unsaturated cyclic structure. At elevated temperatures or in electrochemical reduction during the discharge process it forms a stable surface film on the Li metal surface through ring-opening polymerization.[51,64,125,153,154] It must be pointed out that the Li cycling efficiency at low temperature (0 °C) decreases by adding VC to the EC/Ethyl Methyl Carbonate (EMC) (1 : 1) electrolyte because of poor Li^+ ion migration, which leads to a dendritic morphology of deposited Li and a thicker surface film.[153] In addition, Mogi *et al.* reported that VC does not work well in the $LiClO_4$/PC electrolyte on Li metal.[155] FEC has also been confirmed to significantly improve the Coulombic efficiency of Li anodes. Mogi *et al.* reported that addition of 5% FEC to the $LiClO_4$/PC electrolyte can significantly improve the Coulombic efficiency of Li.[155] They believed that the FEC additive accelerates the rate of electrolyte decomposition, producing a surface film with a uniform structure, which is beneficial for the suppression of dendrite formation. They also observed that the surface film formed in electrolytes containing FEC has lower resistance compared to the pure control electrolyte. Since a high resistance of the surface film is liable to cause a non-uniform current distribution, which accelerates the formation of dendritic Li, a low resistance is one of the important properties required to obtain an effective surface film on Li metal.

(5) Inert additives: in contrast to the 2Me-F and VC-like organic additives discussed above, another type of additive is almost inert to Li metal and forms a stable surface layer on Li anodes through adsorption rather than decomposition/polymerization. These additives include ammonium chlorides with the *n*-alkyl group (*i.e.*, cetyltrimethylammonium chloride),[156] benzene,[150,152,157] and toluene.[157,158] The accumulation of these additives at the electrode/electrolyte interface forms a thin layer which effectively prevents the growth of the resistive passivation layer at the Li surface and thus decreases the interfacial resistance.[150,158]

(6) Metal ions: Matsuda *et al.* found that the Coulombic efficiency of Li electrodes was improved in the electrolyte solutions containing Sn^{4+}, Sn^{2+}, Al^{3+}, In^{3+}, Ga^{3+}, and Bi^{3+} with higher reduction potential than Li.[89,152,159] These inorganic cations will chemically and/or electrochemically deposit to form thin layers of Li alloys on the Li electrode surface. The deposition and alloying preferably take place on the active points/regions of the Li anode surface, leading to increased surface uniformity.[159] Therefore, dendrite formation is greatly suppressed and the Coulombic efficiencies in the charge/discharge cycles are also improved. However, only those alloy layers with low resistance could improve the Coulombic efficiency of Li anode. For example, AlI_3 additive improved the Coulombic efficiency[89,159] but SnI_2 could not since the Li–Sn alloy layer has high resistance.[89] Alkaline or alkaline earth metal ions such as Mg^{2+},[58] K^+,[126] and Na^+[125] have also been adopted to improve the morphology of the deposited Li film. These ions will be reduced prior to Li deposition. Because of the size mismatch between these co-deposited metal and Li atoms, a small amount of co-deposited Mg, K or Na can disrupt Li dendritic growth. Another possibility is that these co-deposited metal ions may react with Li to form an alloy which can potentially be non-dendritic, resulting in a smooth deposit.[125]

(7) Salt additives: lithium bis(oxalato) borate (LiBOB),[55,160,161] lithium difluoro(oxalato)borate (LiDFOB)[162] and lithium tetrafluoro oxalatophosphate (LiTFOP)[163] have been used in Li-ion batteries to improve the stability/cycling efficiency since they can form a dense SEI layer on the electrode surface. These salt additives may have a positive effect on the Li dendrite suppression by enhancing the properties of the SEI film on graphite anodes. It is reasonable to expect that these salt additives may also form a stable SEI film on the Li metal anode and improve its cyclability.

4.2 Li dendrite prevention by *ex situ*-formed surface coating

In addition to *in situ*-formed SEI or alloy layers from the reactions between Li metal and solvents, salts or additives in electrolytes, another approach to suppressing dendrite growth is to cover the Li electrode with an *ex situ*-formed protective layer (or "artificial" SEI layer) by treating Li metal with chosen chemicals prior to its use in battery electrolytes. For example, exposing Li metal to tetraethoxysilane (TEOS)[164] leads to the formation of silica films on Li metal; Fig. 10 shows cross-sectional SEM images of TEOS-protected Li films at different stages of Li deposition/stripping.[164] During the deposition

process, Li is plated back into an empty region that is created beneath the protective layer during Li stripping. Therefore, dendrite growth can be suppressed. The impedance of the surface is essentially unchanged after some 100 cycles of Li plating and stripping.

In addition to treating Li films in TEOS, other coatings such as chlorosilane derivatives[59,165] have been investigated. Choi *et al.* coated the Li metal electrode with a cross-linked gel polymer electrolyte;[166–168] Belov *et al.* protected the Li surface with polyacetylene *via* polymerization.[169] Wu *et al.* modified a Li electrode by exposing it to nitrogen to form a Li_3N layer.[170] These *ex situ*-formed protective layers have good adhesion to and uniform physical contact with the Li surface and acceptable ionic conductivity either intrinsically or formed after soaking in liquid electrolytes. They effectively suppress the reactions between Li metal and the nonaqueous electrolyte, and therefore stabilize the SEI films leading to relatively stable interfacial impedance during cycling/storage. Compared to the *in situ* formed SEI films, the *ex situ* formed films (especially ceramic films such as Li_3N) usually have more defects, are fragile and incapable of self-remedying. Although some of these "artificial" SEI films may be a good protection for Li in the initial state, it is unavoidable that these protective films will be destroyed during cycling or abuse and fresh Li metal will be exposed to electrolytes. The broken SEI layer may lead to significant non-uniformity in the subsequent Li deposition process and accelerate the formation and growth of Li dendrites. This might be one of the main reasons for the sudden capacity fade of rechargeable Li metal batteries with *ex situ* treated Li metal as the anode.

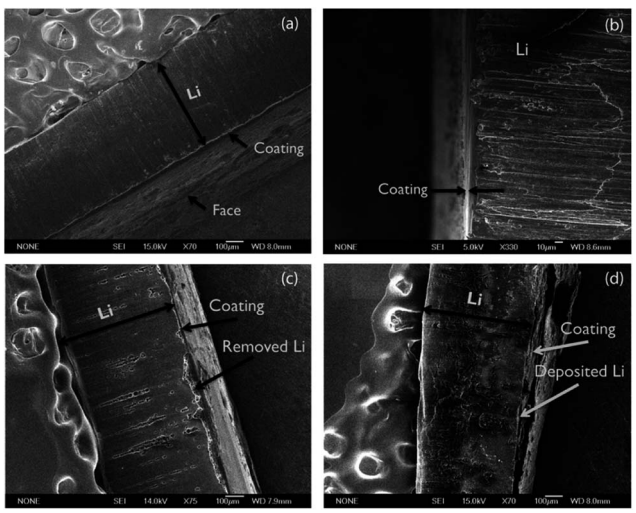

Fig. 10 Cross-sectional SEM micrographs of TEOS-treated Li electrodes. The electrode is imaged at a light angle (~15°) so that it is possible to observe both the cross-section of the Li and the coated Li surface (labelled as "Face"). (a) Li before treatment; (b) higher magnification image of the coating on the Li; (c) TEOS-treated Li after 1000 s of stripping. The gap below the coating is indicated; (d) TEOS-treated Li after 1000 s of stripping followed by 1000 s of plating. The region where the Li has been re-deposited is indicated. The coating is on the order of 1 μm (reproduced with permission.[164] Copyright 2011, Royal Chemical Society).

4.3 Li dendrite prevention by mechanical blocking

As discussed above, Li dendrite growth in liquid electrolytes cannot be prevented even if SEI films formed on Li anodes. This is because Li is thermodynamically unstable with low molecular weight organic solvents and the weak strength of the SEI layers formed in liquid electrolytes. Based on the results of modelling,[11] the dendrite suppression can be achieved if the shear modulus of the electrolyte is about twice that of the Li anode (~10^9 Pa). Compared to liquid electrolytes, polymer electrolytes possess much higher mechanical strength. The effect of polymer electrolytes as mechanical barriers for dendrite prevention will be discussed in this section.

4.3.1 Polymer electrolytes. Generally speaking, any electrolyte containing a macromolecular structure as a part of it can be called a polymer electrolyte (PE). Therefore, this term may refer to a large number of electrolyte systems, which can be divided into classic PEs and hybrid inorganic–organic PEs. Classic PEs include archetypal PEs, plasticized PEs, gel PEs and ionic conducting polyelectrolytes (or single ion conductive polymers). Considering the important effect of the Li^+ transference number on Li dendrites, single ion polymer electrolytes will be discussed separately in Section 4.3.2. Hybrid inorganic–organic PEs cover a wide range of electrolyte systems and can be generally divided into multi-phase PEs and single-phase PEs. It will also be discussed in Section 4.3.3.

Zaghib *et al.* reported that some high molecular weight polymers, such as PEO, are found to be thermodynamically stable with Li even at a high temperature up to 100 °C.[171] There is almost no interfacial reaction between PEO and fresh Li. In this case, Li dendrite growth is the limiting factor that affects the cycle life of Li metal anodes. Therefore, the polymer electrolytes with high shear modulus and excellent stability with fresh Li could overcome the problems related to Li metal anodes and enable the practical applications of rechargeable Li batteries. This is one of the main reasons for the intensive research interest in the development of Li^+-conducting polymer electrolytes during the past three decades.[172–175] Progress in this area has been summarized in several recent reviews.[172,176,177]

Since the original work by Armand *et al.*,[17] PEO and lower molecular weight polyethylene glycol (PEG) with the same chemical structure as PEO have been used as the most common polymer electrolytes in Li metal batteries. PEO has strong solvating properties for Li salts because of complexation by oxygen atoms of ether groups (–CH_2–CH_2–O–) which induces ionic conductivity in the amorphous phase at temperatures of 50–100 °C.[178,179] Solid PEO-based electrolytes have been explored for Li metal battery applications since the 1980s.[17] Although early studies have demonstrated promising cyclabilities in Li metal batteries using PEO-based electrolytes,[180,181] later studies by Scrosati *et al.*[182] and many other groups[183–186] in the late 1980s and early 1990s proved that the dendrite growth cannot be blocked with PEO itself, especially when the batteries operated at elevated temperatures (~80 °C) when the mechanical strength of PEO is significantly reduced. On the other hand, the positive effect of polymer electrolytes on the cycling performance of Li metal batteries was also recognized due to its

excellent chemical stability when in contact with a Li metal anode.

Polar solvents or ILs have often been used to plasticize polymer electrolytes and improve their effectiveness in dendrite prevention. Matsui *et al.* studied a series of poly(ethylene oxide–propylene oxide) (PEO–PPO) copolymers with different molecular weights (M_w) and PEO/PPO ratios as well as different amounts of the added liquid electrolyte (EC–PC) and $LiClO_4$ salt.[183] This systematic investigation revealed that a higher M_w (>16 000) and a PEO/PPO ratio of <5 resulted in elastic polymer electrolyte layers with good liquid-retaining properties, even containing 50–70 wt% liquid electrolyte with 1 M $LiClO_4$. The layers with lower molecular weights were brittle, and as a result the liquid electrolyte leaked where there were cracks and Li dendrites grew in such places.

Another class of polymer electrolytes representing the combination of conventional liquid electrolytes and inert polymer networks is called gel polymer electrolytes (GPEs). In this case, the polymer does not coordinate with Li^+ ions and hence does not contribute to the ionic conductivity. These electrolytes have high ionic conductivity values close to those of liquid electrolytes. On the other hand, good mechanical properties of polymers enable preparation of free-standing films.[187] Some of these electrolyte systems have been successfully applied in dendrite protection.[188–190] For example, *in situ* SEM shows that 5–10 wt% of poly(acrylonitrile) (PAN) in the electrolyte is optimal for dendrite growth suppression.[188] Eichinger *et al.* found that the addition of PAN to the PC–EC electrolyte with either LiTFSI or $LiPF_6$ salt decreased the conductivity but significantly improved the lifetime of a Li battery to 450 cycles.[191] However, such PAN-based gel electrolytes with lower PAN concentrations suffered from reduced mechanical strength, while higher PAN concentrations resulted in increased bulk and interfacial resistance because PAN slowly reacts with Li and forms an interfacial layer with higher resistance. Moreover, the conventional liquid electrolyte components in GPEs make them still thermodynamically incompatible with fresh Li metal.

Mechanical properties of PEO can also be enhanced by using cross-linked polymer networks.[192,193] Tigelaar *et al.* prepared a series of PEO-based electrolytes with addition of pyrrolidinium ILs and by sol–gel cross-linking with triazine linkages employing (3-aminopropyl)triethoxysilane (APTES) chemistry. These APTES cross-linked hyperbranched polymers were found to have higher Li^+ conductivity compared to conventional high molecular weight PEO electrolytes (with the addition of IL) because of their amorphous nature. Li plating/stripping appeared to be highly reversible in the symmetrical Li/Li cells with the prepared cross-linked PE.

Block copolymers that are used in electrolytes for Li batteries consist of a soft block forming Li^+-conducting channels and a hard block forming a rigid network providing mechanical strength against dendrite growth.[194–198] Most of the recent developments are related to the block copolymers of PEO and polystyrene (PS).[199–211] Based on the idea of block copolymer electrolytes, Balsara *et al.* of Seeo Inc. developed a new generation of rechargeable Li batteries based on a proprietary, nanostructured non-flammable PE called DryLyte™.[19] This electrolyte used a block copolymer with a high shear modulus (>10^9 Pa, which is the shear modulus of Li) as a hard matrix for mechanical support. Nanochannels (~10 nm) of polymers (such as PEO, which exhibits a small shear modulus (≪10^9 Pa) but high ionic conductivity) are embedded inside the block copolymer to conduct Li ions. Considering that Li dendrites exhibit a typical size of ~μm, it will be blocked by block copolymers, but Li ions can still transport through narrower ion conducting channels. Therefore, these new PEs can effectively prevent Li dendrite growth. Due to the low ionic conductivities of the polymer-based electrolytes, their application temperatures in Li batteries are at least over 60 °C (the melting point of PEO) and normally at about 80–90 °C, which may be suitable for stationary applications but will be more difficult for transportation applications.

4.3.2 Polymeric single ion conductors. The transference number of Li^+ (t_{Li^+}) has a great impact on the electrochemical performances of rechargeable Li batteries. According to Monroe and Newman's simulations,[33] even at relatively high charge current, no concentration gradients exist in the solution phase and the utilization of active materials remains *ca.* 100% when t_{Li^+} approaches unity. Sand's time τ as shown in eqn (3), which theoretically defines the start time of Li dendrite formation, is proportional to $1/t_{anion}$.[2] For a binary Li ion electrolyte, $t_{anion} + t_{Li^+} = 1$. t_{Li^+} approaching unity means that t_{anion} is small and the Sand's time can become large. Moreover, t_{Li^+} approaching unity means μ_a is close to zero and Li dendrite growth theoretically stops as indicated by eqn (4) and (5). The results of modelling indicate that in the electrolyte with $t_{Li^+} = 1$ it is impossible to form Li dendrites; even if the dendrites formed due to local fluctuations, $\mu_a \rightarrow$ zero means that the dendrite growth rate will be infinitely small. In other words, when t_{Li^+} is unity, Li metal can theoretically be reversibly plated and stripped in the electrolytes. However, in the traditional liquid electrolytes, the t_{Li^+} is less than 0.5. It is even worse at this point for a regular PEO polymer electrolyte with t_{Li^+} *ca.* 0.3. However, the addition of nano-particle fillers, for example TiO_2 or SiO_2, can enhance t_{Li^+} to close to 0.6.[212]

The strategy to increase the Li-ion transference number is to graft the anion on the backbone of the polymer chain, that is, to form a single ion conductor, which was reported as early as 1983, where t_{Li^+} approaches unity as the mobility of the anion is close to zero. In a subsequent study, Sadoway *et al.* introduced Li^+ as a part of a block copolymer with the help of Li methacrylate in order to increase the Li^+ transference number.[213] Poly(lauryl methacrylate-*r*-Li methacrylate)-*b*-poly(oligo(oxyethylene) methacrylate) (P(LMA-*r*-LiMA)-*b*-POEM) with the molar ratio of 1 : 1 : 1 was prepared. Its Li^+ transference number is 0.9, which is twice as high as that for the $LiCF_3SO_3$-containing electrolyte, while the conductivity remained the same. Incorporation of anions into the conducting block, *i.e.*, PLMA-*b*-P(LiMA-*r*-OEM), resulted in a significant decrease of conductivity by one to two orders of magnitude compared to P(LMA-*r*-LiMA)-*b*-POEM and PLMA-*b*-PLiMA-*b*-POEM electrolytes; this was explained by ion dissociation and Li^+ migration to POEM in the latter two cases, while in the former case Li^+ ions stayed

immobile.[214] Interestingly, addition of a Lewis acid (BF_3) increased the conductivity of PLMA-*b*-P(LiMA-*r*-OEM) to the same value as that of the other two electrolytes by the formation of $-COOBF_3^-$, favoring Li^+ dissociation. In a separate effort, Allcock *et al.*[215–217] used amphiphilic single-ion conductive polynorbornenes with pendent cyclotriphosphazenes as lithium-ion conductive membranes for lithium–seawater batteries. However, like many other inorganic ceramics, these polymers cannot be sustainable in strong acid or base solutions for long time, which also limits their practical application in PLEs.

Recently, Armand *et al.* made a breakthrough in the search for single ion polymer conductors.[218] They synthesized a new single ion polymer electrolyte *via* self-assembled polyanionic BAB triblock copolymers as shown in Fig. 11. The B block is a polyelectrolyte based on poly(styrene trifluoromethanesulphonylimide of lithium) (P(STFSILi)) associated with a central A block based on linear poly(ethylene oxide) (PEO). These polymer electrolytes exhibit a mechanical strength much higher than that of PEO and about one order of magnitude higher than that of the PS–PEO–PS copolymer electrolyte, which was expected to mitigate the dendritic Li growth. The ionic conductivity of this polymer electrolyte has reached 1.3×10^{-5} S cm^{-1} at 60 °C which is almost five times that of the state-of-the-art value previously reported for a single ion polymer conductor. The BAB copolymer exhibits a t_{Li^+} exceeding 0.85 and a wide electrochemical stability window up to 5 V (*vs.* Li/Li^+). The polymer Li battery with the $LiFePO_4$ cathode and the BAB copolymer electrolyte demonstrated excellent cycling stability and good power rate. These results demonstrate the importance of the single ion polymer conductors for long term operation of rechargeable Li batteries.

4.3.3 Inorganic–organic hybrid electrolytes. To reinforce the mechanical strength of traditional polymer electrolytes, inorganic fillers, mainly silica particles, were added.[18,219–221] In one of the early studies by Li *et al.* on a Li/V_3O_{13} cell with the gel PEG-based electrolyte,[18] addition of 10 wt% fumed silica particles significantly improved the mechanical properties because of the aggregation of silica particles and the formation of a cross-linked structure. As a result, the elastic modulus increased to that of solids ($G' > 10^5$ Pa) while the conductivity was maintained at 10^{-3} S cm^{-1}. Such a composite electrolyte improved the cycle life compared to the unmodified gel electrolyte. The effect of surface groups on silica was also studied, revealing better electrochemical performance in the case of hydrophilic silica particles. An *in situ* SEM study on the same electrolyte system deduced[219] similar conclusions. 10 wt% of hydrophilic fumed silica in the electrolyte improved the performance, including the cell voltage and cycle life. This effect can be attributed to the formation of a smoother and denser layer as observed by SEM. In addition, it was claimed in this study that silica particles on the Li–polymer electrolyte interface inhibit dendrite formation due to the scavenging of impurities.

Liu *et al.* reported the positive effect of silica particles in the solid PEO electrolyte by electrochemical measurements as well as *in situ* SEM.[220] The delay in the onset time of dendrite formation was attributed to the lower interfacial resistance and slightly higher bulk conductivity in the case of the PEO-based electrolyte modified with acid-treated silica nanoparticles. The same authors further reported the amplification of this electrolyte system by the addition of *N*-methyl-*N*-propylpiperidinium bis(trifluoromethanesulfonyl)imide (PP13TFSI) IL which dramatically increased the onset time of dendrite formation from 15 to 46 h.[221] To support the idea that the electrolyte conductivity and interfacial resistance play an important role in dendrite growth, a comparative study on PEO-based electrolytes with and without IL (PP13TFSI) was carried out by the same group.[38] The dendrite formation was suppressed in the PEO_{18}–LiTFSI–*x*PP13TFSI mixture, where $x = 1.44$, and the corresponding onset time of dendrite formation increased from 15 to 35 h. By using PEO_{18}–LiTFSI–*x*PP13TFSI as the interfacial layer between a Li anode and a glass electrolyte ($Li_{1+x+y}Ti_{2-x}Al_xP_{3-y}Si_yO_{12}$), an aqueous Li–air cell was also fabricated.[222] Low Li deposition and stripping polarization potentials of less than 0.3 V were reported at 0.3 mA cm^{-2} current density compared to 0.6 V without IL. The pronounced effect of IL was attributed to the lower Li/PE interfacial resistance.

The addition of inorganic fillers to liquid electrolytes can also suppress Li dendrite growth. Lu *et al.* reported that the IL-based electrolytes with nano SiO_2 fillers potentially possessed at least two functions to suppress the Li dendrite growth.[223] First, IL molecules dissociated to release cations and anions in the electrolyte, which can migrate to delay/prevent the development of a space charge. Second, the impermeable nanometer-sized particles formed a mechanically strong and highly tortuous interface to retard the penetration of nucleated dendrites. The Li anode after short-circuit by polarization shows the stunted, mushroom-like lithium dendrites.

4.3.4 Inorganic solid state Li-ion conductors. Inorganic solid-state Li-ion conductors are the ideal materials to protect Li against dendrite penetration because of their unity t_{Li^+} and high mechanical strength, which often far exceeds that of Li itself. Both thin films and bulk forms of solid-state Li-ion conductors have been developed to effectively block Li dendrite growth.[224,225] To date, the most widely used inorganic thin film ion conductor is the nitrogen-doped Li-ion phosphate film (LiPON) developed by Bates and Dudney *et al.* in the early

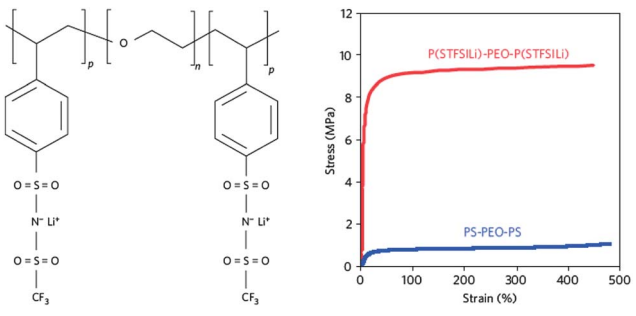

Fig. 11 (a) Chemical structure of the single ion triblock copolymer P(STFSILi)-*b*-PEO-*b*-P(STFSILi); (b) comparison of the tensile stress at 40 °C of P(STFSILi)-*b*-PEO-*b*-P(STFSILi) with 31 wt% P(STFSILi) and PS–PEO–PS with 25 wt% PS loaded with LiTFSI (reproduced with permission.[218] Copyright 2013, Nature).

1990s.[226] LiPON exhibits a conductivity of 2×10^{-6} S cm^{-1} at 25 °C and excellent long-term stability when in contact with Li metal. Bates and Dudney also first reported the application of LiPON as a Li ion conducting electrolyte and Li metal protection layer in a thin film battery.[227] Later on, Herbert and Dudney *et al.*[228] reported that the shear modulus of LiPON is approximately 77 GPa, 7.3 times higher than that of Li, which far exceeds the basic requirement of mechanical strength for electrolytes to suppress the Li dendrites, about twice that of Li. This result is also independent of the substrate type, film thickness, and annealing; therefore, LiPON is expected to be fully capable of mechanically suppressing dendrite formation at the Li/LiPON interface in thin film batteries.

Many different bulk form ceramic glass (~50–200 μm thick) Li-ion conductors were also developed and they can effectively suppress Li dendrite growth. The typical examples of these glass electrolytes include LiSICON-type $Li_{1+x}Al_xTi_{2-x}(PO_4)_3$ (LATP) developed by Fu *et al.*[229,230] and garnet-like oxide glass (Li_6A-$La_2Ta_2O_{12}$ [A = Sr, Ba]) developed by Thangadurai and Weppner.[231] Recently, Wang *et al.* reported a Li|$LiMn_2O_4$ battery operated in an aqueous electrolyte using a Li metal anode protected by LATP glass. The battery demonstrates excellent stability and good electrochemical performance.[232] Another superionic conductor $Li_{10}GeP_2S_{12}$ has been reported recently, which exhibits an extremely high bulk conductivity of over 10^{-2} S cm^{-1} at room temperature (27 °C).[233] However, it is highly sensitive to moisture and unstable when in contact with Li metal. Therefore, it is not used directly with Li anodes.

Among these bulk type ceramic glass materials, LATP glass, developed by Fu of Ohara, Inc. (Japan), has been widely used to protect Li metal glass and applied in Li–air and Li–S batteries, as well as other energy storage and conversion systems. Both LATP glass and garnet type glass are stable in weak acid and alkaline electrolytes. One of the disadvantages of LATP glass is that it is not stable when in contact with Li metal. Visco *et al.* first solved this problem by introducing an interfacial layer (a solid layer such as Cu_3N, LiPON, or nonaqueous electrolyte) between the Li metal and the Ohara glass, thus forming a protected Li electrode (PLE).[21,234,235] Fig. 12(a) shows the schematic of a PLE proposed by Visco *et al.*,[235] where the Li electrode was protected by an interfacial layer and a Li metal phosphate glass. Fig. 12(b) shows a Li–air battery with a double-sided PLE. Li–air batteries using this PLE can operate in both aqueous and nonaqueous electrolytes.[236–239] However, large scale applications of these inorganic solid-state ceramic Li ion conductors are still hindered by their high cost, poor mechanical stability and limited ionic conductivity. Further development of new flexible inorganic solid-state Li-ion conductors with good mechanical strength and stability, high Li ionic conductivity, excellent compatibility with Li metal and wide electrochemical windows is still under investigation for their application in rechargeable Li metal batteries.

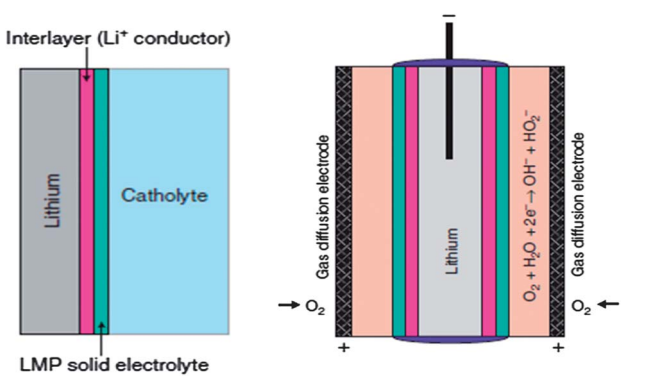

Fig. 12 (a) Use of an interlayer and a water-stable solid electrolyte to protect Li (LMP: Li metal phosphate). (b) Schematic of a Li–air battery based on the PLE technology (reproduced with permission.[235] Copyright 2009, Elsevier).

4.4 Li dendrite prevention by the self-healing electrostatic shield mechanism

As we discussed in the previous sections, various approaches have been used to suppress Li dendrite formation and growth. However, most of these approaches rely on the formation of a strong layer to mechanically block the Li dendrite growth. Recently, we developed a novel mechanism that could influence Li deposition preference to obtain a dendrite-free Li anode, which is called the self-healing electrostatic shield (SHES) mechanism.[240] This mechanism does not rely on the mechanical strength of a protection layer. Instead, it relies on an electrostatic shield formed by electrolyte additives. This layer is positively charged and floats on the tip area of potential dendrites on the surface of the deposited Li film, but does not physically attach to the dendrite and Li film. During the Li deposition process, this electrostatic shield will repel the incoming Li^+ ions and force them to be deposited on the valley area instead of the peak area of the Li film. Once the applied electric voltage is turned off, this charged cloud will dissipate and does not form a permanent film on the Li surface.

Fig. 13 shows the SHES mechanism to prevent Li dendrite formation. According to the Nernst equation, it is possible to find certain metal cations (M^+) that have an effective reduction potential lower than that of Li^+ if the M^+ has a standard redox potential close to Li^+ and a chemical activity much lower than that of Li^+.[240] For example, cesium ions (Cs^+) at a low concentration of 0.01 M have an effective reduction potential of −3.144 V, which is lower than that of Li^+ at 1.0 M concentration (−3.040 V). As a result, in a mixed electrolyte where the additive Cs^+ concentration is much lower than the Li^+ concentration, Cs^+ additives will not be deposited at the Li deposition potential and do not form thin layers of Li alloys at the electrode surface.

As shown in Fig. 13, at the initial stage of deposition, both Li^+ ions and the Cs^+ additive cations are adsorbed on the surface of the substrate (*e.g.*, Li). When the applied voltage (V_a) is slightly lower than the reduction potential of a Li ion (E_{Li/Li^+}) but higher than the reduction potential of the Cs^+ (E_{Cs/Cs^+}), *i.e.* $E_{Li/Li^+} > V_a > E_{Cs/Cs^+}$, then Li gets deposited on the substrate surface (Fig. 13a). Due to the unevenness of the substrate surface or other fluctuations in the system, some Li protuberant tips will unavoidably be formed at the substrate surface (Fig. 13b). Then a higher electron-charge density appears at the newly formed Li

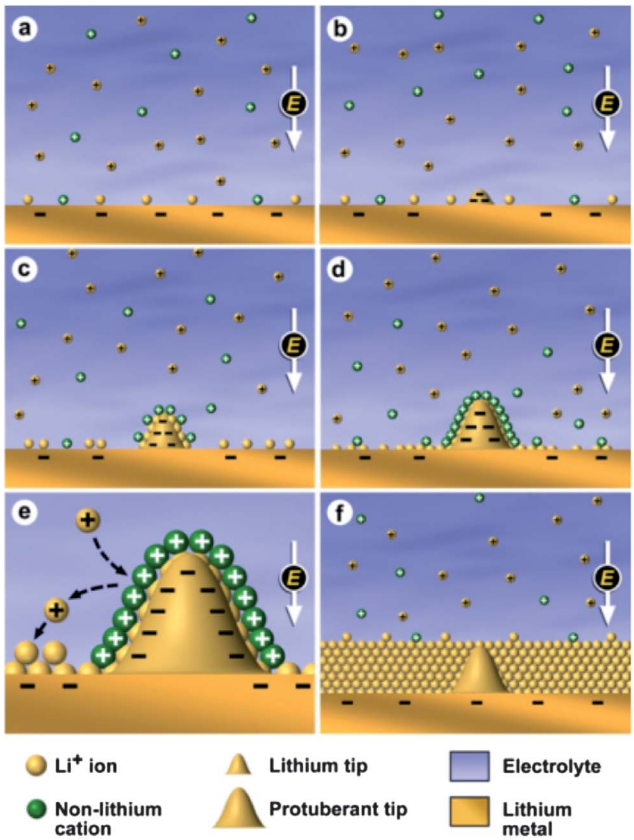

Fig. 13 Illustration of the Li deposition process based on the SHES mechanism (reproduced with permission.[240] Copyright 2013, American Chemical Society).

protuberance that attracts more Li ions from the electrolyte and deposits more on the tip than on other sites, thus forming the Li dendrites as would happen in the conventional electrolytes. However, in the SHES mechanism, more non-Li Cs^+ cations will also be adsorbed on the tip by electrostatic attraction force at the same time (Fig. 13c). When the adsorbed Li ions get deposited on this tip continuously, the number of Li ions around the tip decreases significantly but more and more non-Li cations that could not be electrochemically reduced at this potential will accumulate and surround the tip surface. Then a positively charged electrostatic shield is automatically formed by adsorbed non-Li cations on the Li tip (Fig. 13d). Due to the charge repelling and steric hindrance effect of the non-Li cation shield, it is more difficult for Li ions to adsorb and deposit on such a tip. Li ions have to deposit at other sites with lower non-Li cation adsorption ratios. As a result, the continuous Li growth on this tip (dendrite root) is stopped. It is reasonable to believe that there should be a lot of tips forming on the Li surface, but no tips would grow exceptionally as shown in Fig. 13e. Eventually, a smooth Li surface could be formed as illustrated in Fig. 13f; then this self-healing process will repeat itself. In fact, Fig. 13 is a simplified illustration of a Li deposition process with SHES additives. In practice, a SEI layer will always form on the surface of Li metal once it is in contact with the electrolyte. Therefore, Cs^+ ions will accumulate on the outside of the SEI layer and quickly form an electrostatic shield and prevent amplification of Li dendrite growth.

The SHES additive approach is different from that of inorganic additives (including Mg^{2+}, Al^{3+}, Zn^{2+}, Ga^{3+}, In^{3+}, and Sn^{2+}) used in previous studies.[241,242] These additive metal ions are consumed during each Li deposition and their effectiveness will soon fade with increasing cycles. However, in the proposed SHES mechanism, the additive cations will not be consumed and can last for long-term cycling. This prediction has been verified by chemical analysis of the deposited films.

Fig. 14 shows SEM images of the deposited Li films on copper substrates with different Cs concentrations. In the control electrolyte without the $CsPF_6$ additive, Li dendrite formation is clearly observed in the deposited Li film (see Fig. 14a). Even at very low Cs^+ concentrations (0.005 M), Li dendrite formation is significantly decreased (Fig. 14b). When the Cs^+ concentration is increased to 0.05 M, the dendrite formation is completely eliminated, resulting in a very distinct improvement (Fig. 14c). Further investigation indicated that even if a dendritic Li film was initially formed during Li deposition, it could be smoothened if further deposition was conducted in the electrolyte containing Cs^+ additive. In addition to Cs^+, Rb^+ also exhibits a lower effective reduction potential when its concentration is much lower than that of Li^+. Not surprisingly, $RbPF_6$ was also able to suppress Li dendrite growth although it is not as effective as $CsPF_6$. Unlike other cations, reported in the previous work, that will form part of the SEI layer,[241,242] SHES additives (Cs^+, Rb^+, *etc.*) do not form part of the SEI layer as verified by several trace analysis techniques.[240]

Finally, it is necessary to indicate that although the SHES mechanism has addressed the dendritic morphology problem encountered during Li deposition, the Coulombic efficiency of Li deposition in the electrolytes used in the above work is still relatively low (~76% in the case of 1 M $LiPF_6$/PC). Further optimization of the electrolyte solvents, salts, and additives have increased the Coulombic efficiency of Li deposition/stripping to more than 98% and still retained the dendrite-free morphology of the deposited Li films, which is required for long-term cycling operation of Li metal anodes.

4.5 Li dendrite prevention by other factors

In addition to the strategies discussed above, several other factors, including both sample preparation and testing procedures, may also affect the dendrite growth and cycling life of Li anodes and will be briefly discussed below.

4.5.1 Effect of pressure. Gireaud *et al.*[9] investigated the effect of the morphology of the deposited Li. They found that the Li film deposited at higher pressure is more dense and uniform. This structure change decreased the isolation of the deposited Li and increased the Li cycling efficiency.[9,243] The efficiency of Li deposition rises from 60% to 90% with the pressure increasing from 0.7 kg cm^{-2} to 7 kg cm^{-2}.[9,243] The pressure applied on the cell internal elements confines dendritic Li deposits to the vicinity of the negative electrode and thus enhances the Li cycling efficiency.[9] It needs to be pointed out that applying an external pressure is not always feasible for

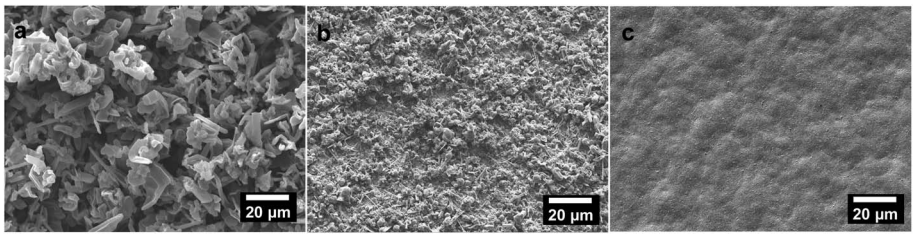

Fig. 14 SEM images of the morphologies of Li films deposited in the 1 M $LiPF_6$/PC electrolyte with $CsPF_6$ concentrations of: (a) 0 M, (b) 0.005 M, (c) 0.05 M, at a current density of 0.1 mA cm^{-2} (reproduced with permission.[240] Copyright 2013, American Chemical Society).

practical power systems such as cylindrical cells and soft package batteries.

4.5.2 Effect of substrate smoothness. In general electrodeposition, the types of substrates and their surface states have significant effects on the morphology of the subsequent deposition. Gireaud *et al.*[9] observed that Li dendritic deposits grow preferentially on metal imperfections such as on the electrochemical stripping fingerprints, which locally enhance the current density (current focalization), leading to dendritic growth from these specific domains. In contrast, smooth and rough surfaces imply a homogeneous current density distribution over the entire Li surface leading to dendrite-free mossy Li deposits. However it remains unknown whether such a non-dendritic morphology could be maintained upon cycling.

4.5.3 Effect of substrate area. As shown in Section 2.2, decreasing the current density is an effective method for slowing down Li dendrite growth. In addition, the charge styles, galvanostatic or pulse, also significantly affect Li dendrite formation and growth. Recent work by Mayers and co-authors reported that pulse charging can effectively suppress Li dendrite formation by as much as 96%.[45] However, the increasing demand for high power batteries makes it impractical to improve the cycle life by simply lowering the deposition/stripping current density. A more practical approach is to increase the effective electrode surface, for example, to adopt Li powder as an anode or a graphene nanosheet as an anode matrix with huge surface area, which would also decrease the effective current density. Zhamu *et al.*[244] have successfully demonstrated that by implementing graphene sheets to increase the anode surface areas, one can significantly reduce the anode current density, thereby dramatically prolonging the dendrite initiation time and decreasing the growth rate of dendrites. One concern is that they used the conventional electrolyte in their work (1 M $LiPF_6$/(EC/DMC in 1 : 1 weight ratio)). The Coulombic efficiency of Li deposition/stripping in this electrolyte is not high (less than 80%) so Li consumption will be a problem for long-term operation of cells unless a large excess of Li metal is used.

5. Summary and perspective

As we discussed above, Li metal is an ideal anode for rechargeable batteries, including Li–air, Li–S, and other Li batteries using intercalation compounds or conversion compounds as cathode materials. Unfortunately, Li dendrite growth and low Coulombic efficiency during the charge/discharge process of Li metal batteries have largely prevented the use of Li metal as an anode for rechargeable batteries. To date, partial solutions for Li dendrite prevention have been identified although they are only effective under certain conditions. For example, the PEO-based block copolymer electrolytes developed by Balsara *et al.*[19,20] can prevent dendrite growth by using the strong shear strength of block copolymers, but these copolymers have to work at elevated temperatures when Li salt–PEO has acceptable conductivities. The new electrolyte additives developed by Ding and Zhang *et al.*[240] can prevent dendrite growth by a self-healing mechanism rather than a physical blocking mechanism, but the existing SHES additives can still only prevent the dendrite growth at limited current densities. Too large a current density will induce a large voltage drop which may force the additives to be deposited with Li and diminish the effect of the additives. Therefore, a more reliable solution still needs to be found to use Li anodes for broad applications. On the other hand, improvement in the Coulombic efficiency of Li deposition/stripping seems to be a more challenging task. Although some electrolytes can lead to a Coulomic efficiency of more than 98%,[117] these electrolytes may not be the best for dendrite prevention. More importantly, as indicated by Whittingham,[1] even if a Coulombic efficiency of 99.9% for Li deposition/stripping can be obtained, at least a threefold excess of Li must be used to retain their initial capacity after 1000 cycles. This will clearly reduce the effective capacities of Li by a factor of three, although these are still much higher than that of a carbon-based anode.

To enable broad applications of Li anodes, more fundamental studies need to be conducted to simultaneously address the two barriers discussed above. Future work also needs to focus more on addressing the origin of the problems instead of only on consequences of the problems. The origins of the Li dendrite formation and growth are the Li^+ concentration gradient during the charge/discharge process and the surface non-uniformity of the deposition. The origin of low Coulombic efficiency is the thermodynamic incompatibility of fresh Li metal with the electrolyte. The results of modelling and simulations anticipate that an electrolyte with high ionic conductivity and a Li^+ transference number close to unity can dramatically alleviate the concentration gradient, which will extend the "Sand's time", *i.e.*, delay or even stop the Li dendrite formation; high shear modulus is also an important property for a functional electrolyte to suppress the Li dendrite growth.

In order to clearly understand the mechanism of Li dendrite formation and growth, various techniques have been adopted to characterize the morphology, components and structures of Li surfaces. Although some *ex situ* techniques give much useful information, Li deposition/stripping is an interfacial reaction so *ex situ* characterization might destroy its original fine morphology. To understand the real dendrite formation and SEI layer formation as well as their interactions, *in situ* or *operando* techniques (including *operando* TEM, SEM, AFM, or *in situ* optical techniques with high magnifications) can provide more information about the local concentration gradient, Li dynamic nucleation and dendritic growth. They can also be used to observe the formation of dendrites and SEI layers at the same time. It is critical to find an ultimate solution to overcome the two barriers that have prevented the application of Li anodes to date.

Although many modelling studies have been done and led to several critical conclusions that guided development of Li metal batteries, most of the modelling work focuses on the physical properties of the dendrite growth. Significant progress in increasing the Coulombic efficiency of Li deposition/stripping (especially Aurbach's work[8,66,67]) is mainly made by experimental efforts. To enable the application of Li anodes, the chemical reactions between Li metal and electrolytes (including both solvents and salts) need to be modeled/simulated to get a better understanding on the formation of the SEI layer and its chemical stability, ionic conductivity, and mechanical flexibility. Furthermore, the interactions between Li dendrites and the SEI layer need to be well understood. For example, when a SHES additive is used, the self-healing behavior will prevent large extrusions of Li dendrites from penetrating the SEI layer. In this case, an SEI layer with limited flexibility will be able to tolerate small variations on the Li surface. This will prevent repeated breakdown/reformation of the SEI layer which is one of the main sources of low Coulombic efficiency that occurs during the operation of a Li anode.

Li is thermodynamically unstable with any organic solvent and they react instantaneously to form an SEI. Therefore, the stability and flexibility of the SEI layer is the most critical factor that determines the performance of a Li metal anode, especially its Coulombic efficiency. The components of the electrolytes, including solvents, Li salts, and additives determine the chemical compositions, ionic conductivity, and mechanical properties of the SEI layer. Compared to liquid electrolytes, polymer materials (especially PEO) present much better compatibility with fresh Li. Therefore, PEO and its derivatives have been extensively investigated for their applications in rechargeable Li metal batteries over the last three decades. However, PEO electrolytes still cannot prevent Li dendrite growth because it has a relatively low ionic conductivity and a small Li^+ transference number, which causes a serious Li^+ concentration gradient during polarization as anticipated by modelling.

An effective strategy is to develop single-ion conductors with a unity Li^+ transference number, plus a strong shear modulus with block copolymers, which dramatically alleviate the concentration gradient and effectively retard the Li dendrite formation and growth. Another possible solution is to combine the self-healing mechanism with an electrolyte that can form a stable SEI layer with Li. The best electrolytes used today with the $CsPF_6$ additive can lead to dendrite-free Li deposition with a Coulombic efficiency of more than 98%. With optimization of the solvent, salt and other additives, it is possible to obtain a dendrite-free Li film with a Coulombic efficiency greater than 99.9%. Further improvement in the conductivity of the electrolyte can reduce the internal voltage drop under a high current density condition.

Practical applications of Li metal anodes for rechargeable batteries may need a combination of different approaches. Most probably, no ideal solution can be found to make a Li anode work under all conditions so different solutions have to be designed for different applications. Although there are still many obstacles to be overcome, we are optimistic that Li metal can be used as an anode in rechargeable batteries in the near future. This will enable wide application of rechargeable Li metal batteries (using intercalation compounds as cathodes), Li–S batteries, and Li–air batteries.

Acknowledgements

This work was supported as part of the Joint Center for Energy Storage Research, an Energy Innovation Hub funded by the U.S. Department of Energy (DOE), Office of Science, Basic Energy Sciences (the fundamental effect of cesium additive); preliminary work on the dendrite prevention was supported by the Assistant Secretary for Energy Efficiency and Renewable Energy, Office of Vehicle Technology of DOE.

References

1 M. S. Whittingham, *Proc. IEEE*, 2012, **100**, 1518–1534.
2 D. Aurbach and Y. Cohen, *J. Electrochem. Soc.*, 1996, **143**, 3525–3532.
3 R. R. Chianelli, *J. Cryst. Growth*, 1976, **34**, 239–244.
4 P. G. Bruce, S. A. Freunberger, L. J. Hardwick and J.-M. Tarascon, *Nat. Mater.*, 2012, **11**, 19–29.
5 X. L. Ji, K. T. Lee and L. F. Nazar, *Nat. Mater.*, 2009, **8**, 500–506.
6 G. Girishkumar, B. McCloskey, A. C. Luntz, S. Swanson and W. Wilcke, *J. Phys. Chem. Lett.*, 2010, **1**, 2193–2203.
7 J.-S. Lee, S. T. Kim, R. Cao, N.-S. Choi, M. Liu, K. T. Lee and J. Cho, *Adv. Energy Mater.*, 2011, **1**, 34–50.
8 D. Aurbach, E. Zinigrad, Y. Cohen and H. Teller, *Solid State Ionics*, 2002, **148**, 405–416.
9 L. Gireaud, S. Grugeon, S. Laruelle, B. Yrieix and J. M. Tarascon, *Electrochem. Commun.*, 2006, **8**, 1639–1649.
10 S. Chandrashekar, N. M. Trease, H. J. Chang, L.-S. Du, C. P. Grey and A. Jerschow, *Nat. Mater.*, 2012, **11**, 311–315.
11 C. Monroe and J. Newman, *J. Electrochem. Soc.*, 2005, **152**, A396–A404.
12 M. Tang, P. Albertus and J. Newman, *J. Electrochem. Soc.*, 2009, **156**, A390–A399.
13 J.-i. Yamaki, S.-i. Tobishima, K. Hayashi, S. Keiichi, Y. Nemoto and M. Arakawa, *J. Power Sources*, 1998, **74**, 219–227.

14 H. Ota, K. Shima, M. Ue and J.-i. Yamaki, *Electrochim. Acta*, 2004, **49**, 565–572.
15 S. Shiraishi, K. Kanamura and Z. i. Takehara, *J. Electrochem. Soc.*, 1999, **146**, 1633–1639.
16 Y. M. Lee, J. E. Seo, Y.-G. Lee, S. H. Lee, K. Y. Cho and J.-K. Park, *Electrochem. Solid-State Lett.*, 2007, **10**, A216–A219.
17 M. B. Armand, M. J. Duclot and P. Rigaud, *Solid State Ionics*, 1981, **3–4**, 429–430.
18 Y. Li, P. S. Fedkiw and S. A. Khan, *Electrochim. Acta*, 2002, **47**, 3853–3861.
19 N. Balsara, http://www1.eere.energy.gov/vehiclesandfuels/pdfs/merit_review_2008/exploratory_battery/merit08_balsara.pdf, 2008.
20 N. P. Balsara, M. Singh, H. B. Eitouni and E. D. Gomez, *US pat.*, application no. 0263725 A1, 2009.
21 S. J. Visco, E. Nimon, L. C. De Jonghe, B. Katz and M. Y. Chu, *IMLB 12 Meeting*, 2004, Abs., p. 396.
22 J. N. Chazalviel, *Phys. Rev. A*, 1990, **42**, 7355–7367.
23 Y. Sawada, A. Dougherty and J. P. Gollub, *Phys. Rev. Lett.*, 1986, **56**, 1260–1263.
24 J. W. Diggle, A. R. Despic and J. O. 'M. Bockris, *J. Electrochem. Soc.*, 1969, **116**, 1503–1514.
25 C. J. Lan, C. Y. Lee and T. S. Chin, *Electrochim. Acta*, 2007, **52**, 5407–54116.
26 L. H. Mendoza-Huízar, C. H. Rios-Reyes and M. G. Gómez-Villegas, *J. Mex. Chem. Soc.*, 2009, **53**, 243–247.
27 O. Aaboubi, J. Douglade, X. Abenaqui, R. Boumedmed and J. VonHoff, *Electrochim. Acta*, 2011, **56**, 7885–7889.
28 K. L. Miyazaki, Y. Shin, T. Fukutsuka and T. Abe, *Electrochemistry*, 2012, **80**, 725–727.
29 M. Rosso, C. Brissot, A. Teyssot, M. Dollé, L. Sannier, J.-M. Tarascon, R. Bouchet and S. Lascaud, *Electrochim. Acta*, 2006, **51**, 5334–5340.
30 C. Brissot, M. Rosso, J. N. Chazalviel and S. Lascaud, *J. Power Sources*, 1999, **81–82**, 925–929.
31 C. Brissot, M. Rosso, J. N. Chazalviel, P. Baudry and S. Lascaud, *Electrochim. Acta*, 1998, **43**, 1569–1574.
32 C. Brissot, M. Rosso, J. N. Chazalviel and S. Lascaud, *J. Electrochem. Soc.*, 1999, **146**, 4393–4400.
33 C. Monroe and J. Newman, *J. Electrochem. Soc.*, 2003, **150**, A1377–A1384.
34 J. L. Barton and J. O. M. Bockris, *Proc. R. Soc. London, Ser. A*, 1962, **268**, 485.
35 M. Rosso, T. Gobron, C. Brissot, J. N. Chazalviel and S. Lascaud, *J. Power Sources*, 2001, **97–98**, 804–806.
36 R. Bhattacharyya, B. Key, H. Chen, A. S. Best, A. F. Hollenkamp and C. P. Grey, *Nat. Mater.*, 2010, **9**, 504.
37 J.-i. Yamaki, *J. Power Sources*, 1998, **74**, 219–227.
38 S. Liu, N. Imanishi, T. Zhang, A. Hirano, Y. Takeda, O. Yamamoto and J. Yang, *J. Electrochem. Soc.*, 2010, **157**, A1092–A1098.
39 K. Kanamura, S. Shiraishi and Z. i. Takehara, *J. Electrochem. Soc.*, 1996, **143**, 2187–2197.
40 D. Aurbach, E. Zinigrad, H. Teller and P. Dan, *J. Electrochem. Soc.*, 2000, **147**, 1274–1279.
41 E. Zinigrad, D. Aurbach and P. Dan, *Electrochim. Acta*, 2001, **46**, 1863–1869.
42 X. Wang, E. Yasukawa and S. Kasuya, *J. Electrochem. Soc.*, 2000, **147**, 2421–2426.
43 O. Crowther and A. C. West, *J. Electrochem. Soc.*, 2008, **155**, A806–A811.
44 A. Teyssot, C. Belhomme, R. Bouchet, M. Rosso, S. Lascaud and M. Armand, *J. Electroanal. Chem.*, 2005, **584**, 70–74.
45 M. Z. Mayers, J. W. Kaminski and T. F. Miller, *J. Phys. Chem. C*, 2012, **116**, 26214–26221.
46 J. O. Besenhard, J. Gürtler, P. Komenda and A. Paxinos, *J. Power Sources*, 1987, **20**, 253–258.
47 D. Aurbach, I. Weissman, A. Zaban and O. Chusid, *Electrochim. Acta*, 1994, **39**, 51–71.
48 K. Kanamura, H. Tamura, S. Shiraishi and Z.-i. Takehara, *J. Electroanal. Chem.*, 1995, **394**, 49–62.
49 H. Ota, X. Wang and E. Yasukawa, *J. Electrochem. Soc.*, 2004, **151**, A427–A436.
50 C. M. López, J. T. Vaughey and D. W. Dees, *J. Electrochem. Soc.*, 2009, **156**, A726–A729.
51 J. K. Stark, Y. Ding and P. A. Kohl, *J. Electrochem. Soc.*, 2011, **158**, A1100–A1105.
52 D. Aurbach, O. Youngman, Y. Gofer and A. Meitav, *Electrochim. Acta*, 1990, **35**, 625–638.
53 D. Aurbach, O. Youngman and P. Dan, *Electrochim. Acta*, 1990, **35**, 639–655.
54 K. Naoi, M. Mori, Y. Naruoka, W. M. Lamanna and R. Atanasoski, *J. Electrochem. Soc.*, 1999, **146**, 462–469.
55 L. Yang, C. Smith, C. Patrissi, C. R. Schumacher and B. L. Lucht, *J. Power Sources*, 2008, **185**, 1359–1366.
56 T. Fujieda, N. Yamamoto, K. Saito, T. Ishibashi, M. Honjo, S. Koike, N. Wakabayashi and S. Higuchi, *J. Power Sources*, 1994, **52**, 197–200.
57 T. Osaka, T. Momma, Y. Matsumoto and Y. Uchida, *J. Electrochem. Soc.*, 1997, **144**, 1709–1713.
58 S. Yoon, J. Lee, S.-O. Kim and H.-J. Sohn, *Electrochim. Acta*, 2008, **53**, 2501–2506.
59 R. S. Thompson, D. J. Schroeder, C. M. López, S. Neuhold and J. T. Vaughey, *Electrochem. Commun.*, 2011, **13**, 1369–1372.
60 F. Orsini, A. Du Pasquier, B. Beaudoin, J. M. Tarascon, M. Trentin, N. Langenhuizen, E. De Beer and P. Notten, *J. Power Sources*, 1998, **76**, 19–29.
61 F. Orsini, A. du Pasquier, B. Beaudouin, J. M. Tarascon, M. Trentin, N. Langenhuizen, E. de Beer and P. Notten, *J. Power Sources*, 1999, **81–82**, 918–921.
62 H. Sano, H. Sakaebe and H. Matsumoto, *J. Power Sources*, 2011, **196**, 6663–6669.
63 P. C. Howlett, D. R. MacFarlane and A. F. Hollenkamp, *Electrochem. Solid-State Lett.*, 2004, **7**, A97–A101.
64 G. H. Lane, A. S. Best, D. R. MacFarlane, M. Forsyth and A. F. Hollenkamp, *Electrochim. Acta*, 2010, **55**, 2210–2215.
65 K.-i. Morigaki and A. Ohta, *J. Power Sources*, 1998, **76**, 159–166.
66 D. Aurbach, B. Markovsky, M. D. Levi, E. Levi, A. Schechter, M. Moshkovich and Y. Cohen, *J. Power Sources*, 1999, **81–82**, 95–111.
67 Y. S. Cohen, Y. Cohen and D. Aurbach, *J. Phys. Chem. B*, 2000, **104**, 12282–12291.

68 K.-i. Morigaki, *J. Power Sources*, 2002, **104**, 13–23.
69 X. H. Liu, L. Zhong, L. Q. Zhang, A. Kushima, S. X. Mao, J. Li, Z. Z. Ye, J. P. Sullivan and J. Y. Huang, *Appl. Phys. Lett.*, 2011, **98**, 183107.
70 H. Ghassemi, M. Au, N. Chen, P. A. Heiden and R. S. Yassar, *Appl. Phys. Lett.*, 2011, **99**(12), 123113-1–123113-3.
71 E. Peled, *J. Electrochem. Soc.*, 1979, **126**, 2047–2051.
72 D. Aurbach, M. L. Daroux, P. W. Faguy and E. Yeager, *J. Electrochem. Soc.*, 1987, **134**, 1611–1620.
73 D. Aurbach, A. Zaban, Y. Ein-Eli, I. Weissman, O. Chusid, B. Markovsky, M. Levi, E. Levi, A. Schechter and E. Granot, *J. Power Sources*, 1997, **68**, 91–98.
74 D. Aurbach, A. Zaban, Y. Gofer, Y. E. Ely, I. Weissman, O. Chusid and O. Abramson, *J. Power Sources*, 1995, **54**, 76–84.
75 K. Kanamura, H. Takezawa, S. Shiraishi and Z. i. Takehara, *J. Electrochem. Soc.*, 1997, **144**, 1900–1906.
76 D. Aurbach, M. Daroux, G. McDougall and E. B. Yeager, *J. Electroanal. Chem.*, 1993, **358**, 63–76.
77 K. Kanamura, H. Tamura, S. Shiraishi and Z. i. Takehara, *J. Electrochem. Soc.*, 1995, **142**, 340–347.
78 M. Odziemkowski, M. Krell and D. E. Irish, *J. Electrochem. Soc.*, 1992, **139**, 3052–3063.
79 I. Rey, J. L. Bruneel, J. Grondin, L. Servant and J. C. Lassègues, *J. Electrochem. Soc.*, 1998, **145**, 3034–3042.
80 I. Rey, J. C. Lassègues, P. Baudry and H. Majastre, *Electrochim. Acta*, 1998, **43**, 1539–1544.
81 P. C. Howlett, D. R. MacFarlane and A. F. Hollenkamp, *J. Power Sources*, 2003, **114**, 277–284.
82 C. Naudin, J. L. Bruneel, M. Chami, B. Desbat, J. Grondin, J. C. Lassègues and L. Servant, *J. Power Sources*, 2003, **124**, 518–525.
83 A. Kominato, E. Yasukawa, N. Sato, T. Ijuuin, H. Asahina and S. Mori, *J. Power Sources*, 1997, **68**, 471–475.
84 G. Nazri and R. H. Muller, *J. Electrochem. Soc.*, 1985, **132**, 2050–2054.
85 G. Nazri and R. H. Muller, *J. Electrochem. Soc.*, 1985, **132**, 1385–1387.
86 G. Nazri and R. H. Muller, *J. Electrochem. Soc.*, 1985, **132**, 2054–2058.
87 H. Ota, Y. Sakata, X. Wang, J. Sasahara and E. Yasukawa, *J. Electrochem. Soc.*, 2004, **151**, A437.
88 Y. Matsuda, M. Ishikawa, S. Yoshitake and M. Morita, *J. Power Sources*, 1995, **54**, 301–305.
89 M. Ishikawa, M. Morita and Y. Matsuda, *J. Power Sources*, 1997, **68**, 501–505.
90 G. M. Stone, S. A. Mullin, A. A. Teran, D. T. Hallinan Jr, A. M. Minor, A. Hexemer and N. P. Balsara, *J. Electrochem. Soc.*, 2012, A222–A227.
91 E. Peled, *J. Power Sources*, 1983, **9**, 253–266.
92 E. Peled, D. Golodnitsky, C. Menachem and D. Bar-Tow, *J. Electrochem. Soc.*, 1998, **145**, 3482–3486.
93 C. M. López, J. T. Vaughey and D. W. Dees, *J. Electrochem. Soc.*, 2009, **156**, A726.
94 K. Nishikawa, T. Mori, T. Nishida, Y. Fukunaka, M. Rosso and T. Homma, *J. Electrochem. Soc.*, 2010, **157**, A1212–A1217.
95 D. Aurbach and A. Zaban, *J. Electroanal. Chem.*, 1994, **367**, 15–25.
96 S.-P. Kim, A. C. T. v. Duin and V. B. Shenoy, *J. Power Sources*, 2011, **196**, 8590–8597.
97 K. Xu, *Chem. Rev.*, 2004, **104**, 4303–4417.
98 D. Aurbach and H. Gottlieb, *Electrochim. Acta*, 1989, **34**, 141–156.
99 D. Aurbach, *J. Electrochem. Soc.*, 1996, **143**, 3809.
100 A. Schechter, D. Aurbach and H. Cohen, *Langmuir*, 1999, **15**, 3334–3342.
101 K. Xu, N. D. Day and C. A. Angell, *J. Electrochem. Soc.*, 1996, **143**, L209–L211.
102 F. M. Delnick, *J. Power Sources*, 1989, **26**, 129–138.
103 D. Aurbach, *J. Power Sources*, 2000, **89**, 206–218.
104 R. Selim and P. Bro, *J. Electrochem. Soc.*, 1974, **121**, 1457–1459.
105 R. D. Rauh and S. B. Brummer, *Electrochim. Acta*, 1977, **22**, 75–83.
106 R. D. Rauh, T. F. Reise and S. B. Brummer, *J. Electrochem. Soc.*, 1978, **125**, 186–190.
107 V. R. Koch and J. H. Young, *J. Electrochem. Soc.*, 1978, **125**, 1371–1377.
108 V. R. Koch, *J. Electrochem. Soc.*, 1979, **126**, 181–187.
109 V. R. Koch, J. L. Goldman, C. J. Mattos and M. Mulvaney, *J. Electrochem. Soc.*, 1982, **129**, 1–4.
110 V. R. Koch and J. H. Young, *Science*, 1979, **204**, 499–501.
111 J. L. Goldman, R. M. Mank, J. H. Young and V. R. Koch, *J. Electrochem. Soc.*, 1980, **127**, 1461–1467.
112 C. D. Desjardins, T. G. Cadger, R. S. Salter, G. Donaldson and E. J. Casey, *J. Electrochem. Soc.*, 1985, **132**, 529–533.
113 J. S. Foos and J. McVeigh, *J. Electrochem. Soc.*, 1983, **130**, 628–630.
114 J. S. Foos and T. J. Stolki, *J. Electrochem. Soc.*, 1988, **135**, 2769–2771.
115 K. M. Abraham, J. L. Goldman and D. L. Natwig, *J. Electrochem. Soc.*, 1982, **129**, 2404–2409.
116 D. Aurbach and E. Granot, *Electrochim. Acta*, 1997, **42**, 697–718.
117 Y. Gofer, M. Ben-Zion and D. Aurbach, *J. Power Sources*, 1992, **39**, 163–178.
118 P. Dan, E. Mengeritski, Y. Geronov, D. Aurbach and I. Weisman, *J. Power Sources*, 1995, **54**, 143–145.
119 E. Mengeritsky, P. Dan, I. Weissman, A. Zaban and D. Aurbach, *J. Electrochem. Soc.*, 1996, **143**, 2110–2116.
120 P. Dan, E. Mengeritsky, D. Aurbach, I. Weissman and E. Zinigrad, *J. Power Sources*, 1997, **68**, 443–447.
121 N. Byrne, P. C. Howlett, D. R. MacFarlane and M. Forsyth, *Adv. Mater.*, 2005, **17**, 2497–2501.
122 J. Xu, J. Yang, Y. NuLi, J. Wang and Z. Zhang, *J. Power Sources*, 2006, **160**, 621–626.
123 K. P. Doyle, C. M. Lang, K. Kim and P. A. Kohl, *J. Electrochem. Soc.*, 2006, **153**, A1353–A1357.
124 G. H. Lane, P. M. Bayley, B. R. Clare, A. S. Best, D. R. MacFarlane, M. Forsyth and A. F. Hollenkamp, *J. Phys. Chem. C*, 2010, **114**, 21775–21785.
125 J. K. Stark, Y. Ding and P. A. Kohl, *J. Electrochem. Soc.*, 2011, **158**, A1100.

126 J. A. Vega, J. Zhou and P. A. Kohl, *J. Electrochem. Soc.*, 2009, **156**, A253.
127 F. W. Dampier, *J. Electrochem. Soc.*, 1981, **128**, 2501–2506.
128 K. M. Abraham, D. M. Pasquariello and F. J. Martin, *J. Electrochem. Soc.*, 1986, **133**, 661–666.
129 I. Yoshimatsu, T. Hirai and J. i. Yamaki, *J. Electrochem. Soc.*, 1988, **135**, 2422–2427.
130 J. T. Dudley, D. P. Wilkinson, G. Thomas, R. LeVae, S. Woo, H. Blom, C. Horvath, M. W. Juzkow, B. Denis, P. Juric, P. Aghakian and J. R. Dahn, *J. Power Sources*, 1991, **35**, 59–82.
131 K. M. Abraham, *J. Power Sources*, 1985, **14**, 179–191.
132 M. Hughes, N. A. Hampson and S. A. G. R. Karunathilaka, *J. Power Sources*, 1984, **12**, 83–144.
133 Y. Matsuda, *J. Power Sources*, 1987, **20**, 19–26.
134 A. Zaban and D. Aurbach, *J. Power Sources*, 1995, **54**, 289–295.
135 D. Aurbach and A. Zaban, *J. Electroanal. Chem.*, 1993, **348**, 155–179.
136 S.-K. Jeong, H.-Y. Seo, D.-H. Kim, H.-K. Han, J.-G. Kim, Y. B. Lee, Y. Iriyama, T. Abe and Z. Ogumi, *Electrochem. Commun.*, 2008, **10**, 635–638.
137 L. Suo, Y. Hu, H. Li, M. Armand and L. Chen, *Nat. Commun.*, 2013, **4**, 1481.
138 D. Aurbach, Y. Gofer, M. Ben-Zion and P. Aped, *J. Electroanal. Chem.*, 1992, **339**, 451–471.
139 Y. Ein-Eli and D. Aurbach, *J. Power Sources*, 1995, **54**, 281–288.
140 D. E. Irish, Z. Deng and M. Odziemkowski, *J. Power Sources*, 1995, **54**, 28–33.
141 D. Aurbach and A. Zaban, *J. Electrochem. Soc.*, 1994, **141**, 1808–1819.
142 J. O. Besenhard, M. W. Wagner, M. Winter, A. D. Jannakoudakis, P. D. Jannakoudakis and E. Theodoridou, *J. Power Sources*, 1993, **44**, 413–420.
143 T. Osaka, T. Momma, Y. Matsumoto and Y. Uchida, *J. Power Sources*, 1997, **68**, 497–500.
144 J. N. Butler, D. R. Cogley and J. C. Synnott, *J. Phys. Chem.*, 1969, **73**, 4026–4027.
145 K. Kanamura, S. Shiraishi and Z. i. Takehara, *J. Electrochem. Soc.*, 1994, **141**, L108–L110.
146 S. Shiraishi, K. Kanamura and Z.-i. Takehara, *Langmuir*, 1997, **13**, 3542–3549.
147 Z.-i. Takehara, *J. Power Sources*, 1997, **68**, 82–86.
148 K. M. Abraham, J. S. Foos and J. L. Goldman, *J. Electrochem. Soc.*, 1984, **131**, 2197–2199.
149 A. O. Bedenbaugh, J. H. Bedenbaugh, J. D. Adkins and W. A. Bergin, *J. Org. Chem.*, 1970, **35**, 543–545.
150 M. Morita, S. Aoki and Y. Matsuda, *Electrochim. Acta*, 1992, **37**, 119–123.
151 Y. Matsuda and M. Sekiya, *J. Power Sources*, 1999, **81–82**, 759–761.
152 Y. Matsuda, *J. Power Sources*, 1993, **43**, 1–7.
153 H. Ota, Y. Sakata, Y. Otake, K. Shima, M. Ue and J.-i. Yamaki, *J. Electrochem. Soc.*, 2004, **151**, A1778–A1788.
154 H. Sano, H. Sakaebe and H. Matsumoto, *J. Electrochem. Soc.*, 2011, **158**, A316–A321.
155 R. Mogi, M. Inaba, S.-K. Jeong, Y. Iriyama, T. Abe and Z. Ogumi, *J. Electrochem. Soc.*, 2002, **149**, A1578–A1583.
156 T. Hirai, I. Yoshimatsu and J. i. Yamaki, *J. Electrochem. Soc.*, 1994, **141**, 2300–2305.
157 K. Saito, Y. Nemoto, S. Tobishima and J. Yamaki, *J. Power Sources*, 1997, **68**, 476–479.
158 J.-W. Choi, G. Cheruvally, D.-S. Kim, J.-H. Ahn, K.-W. Kim and H.-J. Ahn, *J. Power Sources*, 2008, **183**, 441–445.
159 M. Ishikawa, S. Yoshitake, M. Morita and Y. Matsuda, *J. Electrochem. Soc.*, 1994, **141**, L159–L161.
160 M. Wachtler, M. Wohlfahrt-Mehrens, S. Ströbele, J.-C. Panitz and U. Wietelmann, *J. Appl. Electrochem.*, 2006, **36**, 1199–1206.
161 M.-Q. Li, M.-Z. Qu, X.-Y. He and Z.-L. Yu, *Electrochim. Acta*, 2009, **54**, 4506–4513.
162 Z. Chen, Y. Qin, J. Liu and K. Amine, *Electrochem. Solid-State Lett.*, 2009, **12**, A69–A72.
163 Y. Qin, Z. Chen, J. Liu and K. Amine, *Electrochem. Solid-State Lett.*, 2010, **13**, A11–A14.
164 G. A. Umeda, E. Menke, M. Richard, K. L. Stamm, F. Wudl and B. Dunn, *J. Mater. Chem.*, 2011, **21**, 1593–1599.
165 F. Marchioni, K. Star, E. Menke, T. Buffeteau, L. Servant, B. Dunn and F. Wudl, *Langmuir*, 2007, **23**, 11597–11602.
166 N.-S. Choi, Y. M. Lee, J. H. Park and J.-K. Park, *J. Power Sources*, 2003, **119–121**, 610–616.
167 N.-S. Choi, Y. M. Lee, K. Y. Cho, D.-H. Ko and J.-K. Park, *Electrochem. Commun.*, 2004, **6**, 1238–1242.
168 N.-S. Choi, Y. M. Lee, W. Seol, J. A. Lee and J.-K. Park, *Solid State Ionics*, 2004, **172**, 19–24.
169 D. G. Belov, O. V. Yarmolenko, A. Peng and O. N. Efimov, *Synth. Met.*, 2006, **156**, 745–751.
170 M. Wu, Z. Wen, Y. Liu, X. Wang and L. Huang, *J. Power Sources*, 2011, **196**, 8091–8097.
171 K. Zaghib, M. Armand and M. Gautier, *J. Electrochem. Soc.*, 1998, 3135–3140.
172 J. W. Fergus, *J. Power Sources*, 2010, **195**, 4554–4569.
173 G. Li, Z. Li, P. Zhang, H. Zhang and Y. Wu, *Pure Appl. Chem.*, 2008, **80**, 2553–2563.
174 E. Quartarone and P. Mustarelli, *Chem. Soc. Rev.*, 2011, **40**, 2525–2540.
175 Y. V. Baskakova, O. V. Yarmolenko and O. N. Efimov, *Russ. Chem. Rev.*, 2012, **81**, 367.
176 J. L. Schaefer, Y. Lu, S. S. Moganty, P. Agarwal, N. Jayaprakash and L. A. Archer, *Appl. Nanosci.*, 2011, **2**, 91–109.
177 *Polymer electrolytes: fundamentals and applications*, ed. C. Sequeira and D. Santos, Woodhead Publishing Limited, Oxford, 2010.
178 D. E. Fenton, J. M. Parker and P. V. Wright, *Polymer*, 1973, **14**, 589.
179 D. R. Payne and P. V. Wright, *Polymer*, 1982, **23**, 690–693.
180 F. Bonino, B. Scrosati and A. Selvaggi, *Solid State Ionics*, 1986, **18–19**(Part 2), 1050–1053.
181 M. Gauthier, D. Fauteux, G. Vassort, A. Bélanger, M. Duval, P. Ricoux, J. M. Chabagno, D. Muller, P. Rigaud, M. B. Armand and D. Deroo, *J. Electrochem. Soc.*, 1985, **132**, 1333–1340.

182 B. Scrosati, A. Selvaggi, F. Croce and W. Gang, *J. Power Sources*, 1988, **24**, 287–294.
183 T. Matsui and K. Takeyama, *Electrochim. Acta*, 1995, **40**, 2165–2169.
184 T. Osaka, T. Homma, T. Momma and H. Yarimizu, *J. Electroanal. Chem.*, 1997, **421**, 153–156.
185 E. Peled, D. Golodnitsky, G. Ardel and V. Eshkenazy, *Electrochim. Acta*, 1995, **40**, 2197–2204.
186 R. Xue, H. Huang, X. Huang and L. Chen, *Solid State Ionics*, 1994, **74**, 133–136.
187 K. M. Abraham and M. Alamgir, *J. Electrochem. Soc.*, 1990, **137**, 1657–1658.
188 T. Tatsuma, M. Taguchi, M. Iwaku, T. Sotomura and N. Oyama, *J. Electroanal. Chem.*, 1999, **472**, 142–146.
189 T. Tatsuma, M. Taguchi and N. Oyama, *Electrochim. Acta*, 2001, **46**, 1201–1205.
190 N.-S. Choi, B. Koo, J.-T. Yeon, K. T. Lee and D.-W. Kim, *Electrochim. Acta*, 2011, **56**, 7249–7255.
191 G. Eichinger and M. Fabian, *J. Power Sources*, 1997, **68**, 381–386.
192 D. M. Tigelaar, M. A. B. Meador and W. R. Bennett, *Macromolecules*, 2007, **40**, 4159–4164.
193 T. Itoh, Y. Ichikawa, T. Uno, M. Kubo and O. Yamamoto, *Solid State Ionics*, 2003, **156**, 393–399.
194 D. R. Sadoway, *J. Power Sources*, 2004, **129**, 1–3.
195 P. P. Soo, B. Huang, Y. I. Jang, Y. M. Chiang, D. R. Sadoway and A. M. Mayes, *J. Electrochem. Soc.*, 1999, **146**, 32–37.
196 A.-V. G. Ruzette, P. P. Soo, D. R. Sadoway and A. M. Mayes, *J. Electrochem. Soc.*, 2001, **148**, A537–A543.
197 P. E. Trapa, B. Huang, Y.-Y. Won, D. R. Sadoway and A. M. Mayes, *Electrochem. Solid-State Lett.*, 2002, **5**, A85–A88.
198 A. Ghosh and P. Kofinas, *J. Electrochem. Soc.*, 2008, **155**, A428.
199 T. Niitani, M. Shimada, K. Kawamura, K. Dokko, Y.-H. Rho and K. Kanamura, *Electrochem. Solid-State Lett.*, 2005, **8**, A385–A388.
200 M. Singh, O. Odusanya, G. M. Wilmes, H. B. Eitouni, E. D. Gomez, A. J. Patel, V. L. Chen, M. J. Park, P. Fragouli, H. Iatrou, N. Hadjichristidis, D. Cookson and N. P. Balsara, *Macromolecules*, 2007, **40**, 4578–4585.
201 W.-S. Young, P. J. Brigandi and T. H. Epps, *Macromolecules*, 2008, **41**, 6276–6279.
202 E. D. Gomez, A. Panday, E. H. Feng, V. Chen, G. M. Stone, A. M. Minor, C. Kisielowski, K. H. Downing, O. Borodin, G. D. Smith and N. P. Balsara, *Nano Lett.*, 2009, **9**, 1212–1216.
203 N. S. Wanakule, A. Panday, S. A. Mullin, E. Gann, A. Hexemer and N. P. Balsara, *Macromolecules*, 2009, **42**, 5642–5651.
204 A. Panday, S. Mullin, E. D. Gomez, N. Wanakule, V. L. Chen, A. Hexemer, J. Pople and N. P. Balsara, *Macromolecules*, 2009, **42**, 4632–4637.
205 N. S. Wanakule, J. M. Virgili, A. A. Teran, Z.-G. Wang and N. P. Balsara, *Macromolecules*, 2010, **43**, 8282–8289.
206 I. Choi, H. Ahn and M. J. Park, *Macromolecules*, 2011, **44**, 7327–7334.
207 S. A. Mullin, G. M. Stone, A. Panday and N. P. Balsara, *J. Electrochem. Soc.*, 2011, **158**, A619.
208 F. I. Allen, M. Watanabe, Z. Lee, N. P. Balsara and A. M. Minor, *Ultramicroscopy*, 2011, **111**, 239–244.
209 W.-S. Young, J. N. L. Albert, A. B. Schantz and T. H. Epps, *Macromolecules*, 2011, **44**, 8116–8123.
210 A. A. Teran, S. A. Mullin, D. T. Hallinan and N. P. Balsara, *ACS Macro Lett.*, 2012, **1**, 305–309.
211 W.-S. Young and T. H. Epps, *Macromolecules*, 2012, **45**, 4689–4697.
212 F. Croce, G. B. Appetecchi, L. Persi and B. Scrosati, *Nature*, 1998, **394**, 456–458.
213 D. R. Sadoway, B. Huang, P. E. Trapa, P. P. Soo, P. Bannerjee and A. M. Mayes, *J. Power Sources*, 2001, **97–98**, 621–623.
214 S.-W. Ryu, P. E. Trapa, S. C. Olugebefola, J. A. Gonzalez-Leon, D. R. Sadoway and A. M. Mayes, *J. Electrochem. Soc.*, 2005, **152**, A158–A163.
215 D. T. Welna, D. A. Stone and H. R. Allcock, *Macromolecules*, 2005, **38**, 10406–10412.
216 D. A. Stone, H. R. Allcock and D. T. Welna, *Chem. Mater.*, 2006, 4486–4492.
217 D. T. Welna, H. R. Allcock and D. A. Stone, *Chem. Mater.*, 2007, **19**, 2473–2482.
218 R. Bouchet, S. Maria, R. Meziane, A. Aboulaich, L. Lienafa, J. Bonnet, T. N. Phan, D. Bertin, D. Gigmes, D. Devaux, R. Denoyel and M. Armand, *Nat. Mater.*, 2013, **12**, 452–457.
219 X.-W. Zhang, Y. Li, S. A. Khan and P. S. Fedkiw, *J. Electrochem. Soc.*, 2004, **151**, A1257–A1263.
220 S. Liu, N. Imanishi, T. Zhang, A. Hirano, Y. Takeda, O. Yamamoto and J. Yang, *J. Power Sources*, 2010, **195**, 6847–6853.
221 S. Liu, H. Wang, N. Imanishi, T. Zhang, A. Hirano, Y. Takeda, O. Yamamoto and J. Yang, *J. Power Sources*, 2011, **196**, 7681–7686.
222 T. Zhang, N. Imanishi, A. Hirano, Y. Takeda and O. Yamamoto, *Electrochem. Solid-State Lett.*, 2011, **14**, A45–A48.
223 Y. Lu, S. K. Das, S. S. Moganty and L. A. Archer, *Adv. Mater.*, 2012, **24**, 4430–4435.
224 J. Christensen, P. Albertus, R. S. Sanchez-Carrera, T. Lohmann, B. Kozinsky, R. Liedtke, J. Ahmed and A. Kojic, *J. Electrochem. Soc.*, 2012, **159**, R1–R30.
225 Y. Shao, F. Ding, J. Xiao, J. Zhang, W. Xu, S. Park, J.-G. Zhang, Y. Wang and J. Liu, *Adv. Funct. Mater.*, 2013, **23**, 987–1004.
226 J. B. Bates, N. J. Dudney, G. R. Gruzalski, R. A. Zuhr, A. Choudhury, C. F. Luck and J. D. Robertson, *J. Power Sources*, 1993, **43**, 103–110.
227 J. B. Bates, *US pat.*, 5314765, 1994.
228 E. G. Herbert, W. E. Tenhaeff, N. J. Dudney and G. M. Pharr, *Thin Solid Films*, 2011, **520**, 413–418.
229 J. Fu, *Solid State Ionics*, 1997, **96**, 195–200.
230 J. Fu, *US Pat.*, 5702995, 1997.
231 V. Thangadurai and W. Weppner, *Adv. Funct. Mater.*, 2005, **15**, 107.
232 X. Wang, Y. Hou, Y. Zhu, Y. Wu and R. Holze, *Sci. Rep.*, 2013, **3**, 1401.

233 N. Kamaya, K. Homma, Y. Yamakawa, M. Hirayama, R. Kanno, M. Yonemura, T. Kamiyama, Y. Kato, S. Hama, K. Kawamoto and A. Mitsui, *Nat. Mater.*, 2011, **10**, 682–686.
234 S. J. Visco and Y. S. Nimon, *US Pat.*, 7645543, 2010.
235 S. J. Visco, E. Nimon, B. Katz, L. C. De Jonghe and M. Y. Chu, *Encyclopedia of Electrochemical Power Sources*, J. Garche, *et al.*, Elsevier, Amsterdam, 2009, Abs., pp. 376–383.
236 T. Zhang, N. Imanishi, Y. Shimonishi, A. Hirano, Y. Takeda, O. Yamamoto and N. Sammes, *Chem. Commun.*, 2010, **46**, 1661–1663.
237 E. Yoo and H. Zhou, *ACS Nano*, 2011, **5**, 3020–3026.
238 L. Li, X. Zhao, Y. Fu and A. Manthiram, *Phys. Chem. Chem. Phys.*, 2012, **14**, 12737–12740.
239 K. Huang, Y. Xing and Y. Li, *Electrochim. Acta*, 2012, **81**, 20–24.
240 F. Ding, W. Xu, G. L. Graff, J. Zhang, M. Sushko, X. Chen, Y. Shao, M. H. Engelhard, Z. Nie, J. Xiao, X. Liu, P. V. Sushko, J. Liu and J.-G. Zhang, *J. Am. Chem. Soc.*, 2013, **135**(11), 4450–4456.
241 Y. Matsuda, M. Morita and H. Nigo, in *Primary and Secondary Lithium Batteries*, ed. K. M. Abraham and M. Salomon, The Electrochemical Society Proceedings Series, Pennington, NJ, 1991, vol. 91–93, p. 272.
242 Y. Matsuda, *J. Power Sources*, 1993, **43**, 1–7.
243 T. Hirai, I. Yoshimatsu and J. i. Yamaki, *J. Electrochem. Soc.*, 1994, **141**, 611–614.
244 A. Zhamu, G. Chen, C. Liu, D. Neff, Q. Fang, Z. Yu, W. Xiong, Y. Wang, X. Wang and B. Z. Jang, *Energy Environ. Sci.*, 2012, **5**, 5701–5707.